One-shot identification of SARS-CoV-2 S RBD escape mutants using yeast screening

Irene Francino Urdaniz[1,#], Paul J. Steiner[1,#], Monica B. Kirby[1,#], Fangzhu Zhao[2], Cyrus M. Haas[1], Shawn Barman[2], Emily R. Rhodes[1], Linghang Peng[2], Kayla G. Sprenger[1], Joseph G. Jardine[3], Timothy A. Whitehead[1,*]

[1]Department of Chemical and Biological Engineering, University of Colorado, Boulder, CO 80305, USA
[2]The Scripps Research Institute, La Jolla, CA, USA
[3]International AIDS Vaccine Initiative, New York, NY, USA

# Co-authors contributed equally.
*Correspondence to:
Timothy A. Whitehead: timothy.whitehead@colorado.edu
JSC Biotechnology Building

3415 Colorado Avenue, Boulder, CO 80305

Phone: +1 (303)-735-2145

One Sentence Summary: We present a facile method to identify antibody escape mutants on SARS-CoV-2 S RBD.

ABSTRACT

The potential emergence of SARS-CoV-2 Spike (S) escape mutants is a threat to reduce the efficacy of existing vaccines and neutralizing antibody (nAb) therapies. An understanding of the antibody/S escape mutations landscape is urgently needed to preemptively address this threat. Here we describe a rapid method to identify escape mutants for nAbs targeting the S receptor binding site. We identified escape mutants for five nAbs, including three from the public germline class VH3-53 elicited by natural COVID-19 infection. Escape mutations predominantly mapped to the periphery of the ACE2 recognition site on the RBD with K417, D420, Y421, F486, and Q493 as notable hotspots. We provide libraries, methods, and software as an openly available community resource to accelerate new therapeutic strategies against SARS-CoV-2.

MAIN

The type I viral fusion protein Spike (S) is a major antigenic determinant of SARS-CoV-2 and is the antigen used in all approved COVID-19 vaccines *(1–3)*. Recently, the B.1.1.7 (N501Y; U.K.), B.1.351 (E484K; South Africa), B.1.427 (L452R; California), and B.1.526 (S477N, E484K; NY) viral lineages have emerged. All encode single nucleotide substitutions in the S receptor binding domain (RBD) near recognition site for its cellular target angiotensin-converting enzyme 2 (ACE2) *(3–5)*.

Dozens of studies have reported the structural, epitopic, and functional landscape of non-neutralizing monoclonal antibodies and nAbs targeting trimeric S *(6–8)*. A prophetic understanding of the mutations on S that could evade antibody recognition would enable development of better vaccine boosters and monoclonal antibody therapies. Thus, we sought to develop an S RBD yeast surface display (YSD) platform (**Fig. S1**) *(9)*, as we hypothesized that broad identification of SARS-CoV-2 S escape mutants could be found by integrating high throughput screening platforms with deep sequencing. While a similar platform uses the loss of nAb binding to identify escape mutants *(10, 11)*, we rationalized that a functional screening assay that directly measures the ability of a nAb to compete with ACE2 for S RBD binding, would be a comparatively strong predictor of RBD escapability, as it accounts for mutations in RBD that would disrupt S binding to ACE2.

We had previously developed an aglycosylated S-RBD YSD platform (S RBD(333-537)-N343Q) *(8)* that can bind specifically to ACE2 (**Fig. 1a**). This S RBD construct has its one native N-linked glycan removed (N343Q) as the heavy N-linked mannosylation endemic of *S. cerevisiae* could hamper anti-S RBD mAb recognition. Cell surface titrations of CR3022 IgG and nAb HKU-910-30 IgG yielded apparent dissociation constants comparable to reported *in vitro* results *(6,8)* (**Fig. S2**). We next tested a panel of eleven additional anti-S RBD mAbs for binding to aglycosylated RBD *(7)*. Ten of the eleven mAbs recognized aglycosylated S RBD (**Fig. 1b**). The one panel member that did not bind, CC6.33, selectively recognizes the S309 epitope on the RBD containing the N-linked glycan at position 343 *(12)*.

Next, we evaluated the ability of the mAb panel to competitively inhibit ACE2 binding to aglycosylated S RBD in an assay conceptually similar to the one previously described by Tan et al. *(13)*. Yeast displaying aglycosylated S RBD was first labeled with a saturating concentration of a given mAb and then co-incubated with biotinylated ACE2. Six mAbs completely ablated ACE2 binding, one mAb partially inhibited ACE2, and the remaining four did not prevent ACE2 binding (**Fig. 1c**). A direct correlation was observed between the previously determined neutralization potency of the antibody *(6, 8)* and the fluorescence signal increase in the competition assay (**Fig. 1c**). We conclude from these experiments that, excluding the S309 epitope, the aglycosylated S RBD platform faithfully recapitulates binding interactions of nAbs with S RBD *(7)*.

Our strategy for identifying potential S RBD escape mutants was as follows. First, we constructed a saturation mutagenesis library of aglycosylated S RBD containing all possible single missense and nonsense mutations for the 119 surface exposed positions of the RBD (96% coverage of the 2,380 possible library members; **Table S1** contains library coverage statistics) *(14)*. We labeled

yeast displaying these RBD variants with a saturating concentration of nAb and then co-incubated with a saturating concentration of biotinylated ACE2. We then used fluorescence activated cell sorting (FACS) to screen for mutants that could bind ACE2, indicating that the RBD mutation allows for evasion of the nAb while not disrupting the ACE2 interaction critical for cell entry **(Fig. 1d, Fig. S3-S4**). Importantly, a control with no ACE2 labeling was sorted to set an empirical false discovery rate (FDR) for putative escape mutant hits (**Fig. 1d, Fig. S4**). Plasmid DNA from sorted cells were prepped and deep sequenced. We determined the enrichment ratio *(15)* for each mutant in the sorted population relative to a reference population, and then used the control population to set the FDR (**Fig. 1e, Fig S5**). We screened five different nAbs identified earlier as having completely ablated ACE2 binding (CC6.29, CC6.31, CC12.1, CC12.3, CC12.13). In all, we identified a total of 97 S RBD mutants that can escape recognition by at least one nAb (**Table S2**).

For all five nAbs, the putative escape mutant hits were localized in specific locations within the S RBD primary sequence (**Fig. 1f, Fig. S6-S10**). CC12.1 and CC12.3 belong to the public germline class VH3-53 *(6 ,8, 16)* and are representative of the subset of VH3-53 public antibodies with relatively short CDRH3 lengths *(17)*. Strikingly, these two nAbs share over 90% of the same RBD escape mutants (**Fig. 1g**), even though the light chain differs between the nAb. Structural complexes of antibodies CC12.1 and CC12.3 were previously solved in complex with S RBD *(18)*, affording a structural basis of individual escape mutants. Escape mutants for both of the VH3-53 nAbs CC12.1 and CC12.3 clustered at the same location on the S RBD mainly peripheral to the ACE2 binding site (**Fig 1h; Fig. S11**).

Having identified a number of putative escape mutants from the mutagenesis library screening we sought to determine how this functional screening correlated with the more conventional pseudovirus neutralization assay. A panel of MLV-based SARS-CoV-2 pseudoviruses were generated that contained single mutations predicted by the mutagenesis scanning to allow escape from one of the antibodies screened, as well as several irrelevant control mutations. Antibodies CC12.1, CC12.3 and CC6.29 were screened against the original SARS-CoV-2 pseudovirus as well as this panel of mutant pseudoviruses in duplicate (**Fig. 1i**), and the resulting IC_{50}s were compared to calculate the effect on antibody neutralization potency (**Fig. 1j; Fig. S12**). Consistent with RBD mutagenesis library and structural analysis, CC6.29 failed to neutralize F486I, E484K, and T478R variants. Additionally, K417N, K417T, and D420K hotspot mutants completely escaped neutralization for both CC12.1 and CC12.3. The only instance we tested where the mutagenesis scanning data differed from the pseudovirus results was at N501Y that was predicted to confer escape from CC12.1 and CC12.3 but had no effect on the *in vitro* neutralization potency. Although it is unclear why this discrepancy occurred, we note that N501Y significantly increases the affinity of RBD for ACE2, which could result in ACE2 competing off bound nAb.

Finally, we performed biological replicates where the mutagenesis library corresponding to S RBD positions 437-537 was separately transformed into yeast and screened against nAbs CC6.29, CC12.1, and CC12.3. While the overall magnitude of the enrichment ratios were lower than in the initial experiment, nearly the same set of escape mutants were identified for CC6.29, and escape mutants originally identified for all nAbs had significantly higher ERs than other variants in the replicate (p-value range 4.2e-4 to 1.9e-11, one-sided Welch's t-test) (**Fig. S13**).

Selected per-position heatmaps, and structural mapping of S RBD escape mutants, are shown in **Fig. 2** for all five nAbs. Closer examination of these datasets reveals key features of the RBD

escape mutant response. CC12.1 and CC12.3 nAbs share over 90% of the same RBD escape mutants (**Fig. 1g**), including notable hotspot mutations occurring at K417, D420, Y421, and Q498 (**Fig. 2a**). Interestingly, multiple aromatic substitutions at Q498 escape recognition for CC12.1 & CC12.3 even though the antibodies have different light chains and recognition motifs for that position. Introduction of an aromatic residue at Q498 introduces substantial van der Waals clashes that are likely unresolved without antibody loop movement. The other VH3-53 nAb tested, CC12.13, has a 15 amino acid length CDRH3 that likely has a distinct binding mode than that for CC12.1 and CC12.3 *(17)*. Consistent with this, the CC12.13 escape mutants identified are mostly different from those for CC12.1/CC12.3 (**Fig. S10**).

Another nAb screened, CC6.29, has a completely different escape mutant profile compared with CC12.1/CC12.3. The 15 potential RBD escape mutants for CC6.29 center around the structural 'knob' of positions A475, S477, T478, E484, and F486 (**Fig. 2b**). E484K shared by the B.1.351 and B.1.526 lineages is identified as an escape mutant for this nAb, but the structurally adjacent S477N mutation newly identified in the B.1.526 lineage does not escape CC6.29 neutralization. Intriguingly, S477P is identified as an escape mutant for this nAb. F486 shows up as a mutational hotspot even though that position is involved in the recognition of ACE2. However, a previous mutational scan of S RBD shows that F486 mutation does not significantly impact ACE2 binding affinity *(10)*. CC6.31 escape mutants partially overlap with CC6.29 but implicate a different set of mutants (**Fig. 2b**). Multiple mutations at Q493 escape CC6.31, including Q493 substitutions to aromatic positions F/W.

In total, the five nAbs map a partially overlapping surface with the ACE2 binding site that is primed for antibody escape. In comparison with the binding footprint of ACE2 **(Fig. 2c)**, the escape mutants almost completely map to the outer binding shell and periphery of the interaction surface, akin to an O ring circumnavigating the receptor binding site. Out of the identified escape mutants, residues K417, F486, Q493, N501, and Y505 are located on the ACE2 footprint (**Fig. 2c**). While mutations on K417 and F486 do not significantly change the RBD affinity to ACE2, mutations on N501 can both increase or decrease affinity depending on the substitution. The Y505W mutant shared by CC6.31, CC12.1, and CC12.3 also increases ACE2 affinity *(10)*.

We puzzled why mutations at D420 were so deleterious to the neutralization potency of the VH3-53 nAbs given that this residue is on the outer periphery of the binding epitope. To obtain insight into this question, we performed 100 ns aqueous molecular dynamics (MD) simulations of CC12.1 and CC12.3 in complex with wildtype S RBD and S RBD incorporated with the D420E, D420K, or the Y421N mutation (see SI for details). In the control simulation with CC12.1, D420 on the RBD and CDRH2 S56 on CC12.1 form persistent hydrogen bonds, and Y421 on the RBD is tightly bound within a pocket of CC12.1 residues (**Fig. 3a**). With the D420E mutation, the increased length of E420 disrupts its ability to hydrogen bond with S56, requiring it to adopt a bent conformation (**Fig. 3b**). This forces Y421 out of the antibody pocket, causing increased fluctuations in neighboring RBD loops which persist throughout the entire 100 ns production simulation (**Fig. S14a, b**). With the D420K mutation, hydrogen bonding with S56 is completely disrupted, and with the Y421N mutation, N421 is too short to interact with the antibody pocket (**Fig. S14c**). Similar escape mechanisms are observed for CC12.3 with all three RBD mutations, including increased fluctuations at one of the same key sites (K458) on the RBD in response to the D420E mutation (**Fig. S14d, e**).

There have been a number of recent approaches to identify specific S escape mutants (summarized in **Table S3**) *(11, 19–22)*. A survey of the existing escape mutant literature, along with escape mutants identified in the present work, allows us to identify the absolute and near-absolute escape resistant ACE2 receptor binding site (RBS) residues in the context of the original lineage (**Fig. 3c**). One resistant patch is found around F456/Y473/N487/Y489 while other residues are discontinuous patches on the remainder of the RBS. We note that many of these same resistant residues are identical to those from SARS-CoV (Y449, N487, Y489, G496, T500 and G502). The lack of a contiguous surface at the RBS that is conserved makes it highly unlikely that one could identify a naïve nAb targeting the RBS that is completely resistant to escape.

A major near-term concern with public health implications are identification of the set of single nucleotide polymorphisms that encode for escape mutants on the S RBD. A summary of 1-nucleotide (nt) escape mutants identified in the present work is shown in **Fig. 3d**. To our knowledge, 22/35 (63%) of 1-nt escape mutants identified from this nAb panel have not previously been identified, including hotspot positions D420 and Y421 that escape recognition by the abundant VH3-53 nAbs. Other notable residues identified here include S477, Q498, and Y501, as these positions lie directly on the receptor binding site and all have been shown to slightly increase binding affinity to ACE2 *(10)*. Mutants E484K and N501Y in currently circulating lineages escape some but not all of the nAbs on the panel.

We have developed a yeast platform that allows for the rapid identification of SARS-CoV-2 S RBD escape mutants for a given nAb. While other platforms to identify escape mutants have recently been described, key advantages of the approach presented here includes: (i.) screening by competitive binding against ACE2 which more precisely mimics how actual viral infection can still persist despite antibody binding; (ii.) a robust and rigorous hit identification algorithm; (iii.) a safe working environment, as it does not use live virus; and (iv.) a relatively fast identification, as the RBD library can be screened against a given nAb and analyzed in under a week. There also exist drawbacks. First, the present method is limited to mapping escape mutants for anti-S-RBD nAbs that directly compete with ACE2 for binding. Many nAbs neutralize by targeting S epitopes across protomers *(23)* or on the N-terminal domain *(24)*, and a robust platform for S ectodomain display would enable more comprehensive studies. We attempted to develop a yeast platform for S ectodomain but were unsuccessful: we screened media composition, expression temperature, protein orientation (**Fig. S15**), and mutations (1,909 mutants screened with only two potential hits) (**Data S2-3, Table S1, Fig. S16**). Second, the presented assay measures the ability of a given mutant to escape nAb blockade of ACE2. While from all available data the assay appears to correlate well in the context of pseudo-virus, each mutation is pleiotropic with unknown fitness effects beyond escape for a given nAb; the true RBS escape mutants that do not appreciably impede viral fitness will be a subset of the mutations identified here.

Still, using this method we were able to identify specific failure mechanisms for five different nAbs. This tool can be easily adapted and contribute to developing the next generation of broadly neutralizing antibodies against SARS-CoV-2, as well as suggest mutations to include for the next generation of vaccines. To that end, it would be interesting to see whether our yeast platform presented here is robust enough to identify escape mutants from bulk sera from convalescent or vaccinated individuals.

Acknowledgements

We thank scientists K. Jackson and A. Scott at the BioFrontiers sequencing core for technical guidance, and members of the Whitehead lab for intellectual and material support, including Matt Bedewitz for reagent prep. The anti-SARS-CoV-2 RBD antibody panel used was a kind gift from Dennis Burton's lab at Scripps, and the ACE2-Fc and CR3022 were kind gifts from Neil King's lab at the University of Washington. **Funding:** Research reported in this publication was supported by the National Institute Of Allergy And Infectious Diseases of the National Institutes of Health under Award Number R01AI141452 to T.A.W. The content is solely the responsibility of the authors and does not necessarily represent the official views of the National Institutes of Health. This research was also supported by a Balsells Fellowship to I.F.U. and a CU Boulder BSI fellowship to C.M.H. **Author Contributions:** Designed experiments: IFU, PJS, MBK, ERR, KGS, JJ, TAW; Performed experiments: IFU, PJS, MBK, SB, LP, FZ, ERR; Performed simulations: ERR, KGS; Developed algorithms and software: PJS, CMH, TAW; Wrote paper: IFU, PJS, MBK, KGS, TAW. **Competing Interests:** IFU, PJS, MBK, CH, JJ, TAW declare competing interests.

Data and Reagent Availability

Raw sequencing reads for this work have been deposited in the SRA (Accession #s SAMN18250431-SAMN18250483). All plasmids and mutational libraries used in this work are available from AddGene (AddGene Collection **To Be Added Upon Publication**). All scripts used to process and analyze deep sequencing data are freely available on Github (https://github.com/WhiteheadGroup/SpikeRBDStabilization.git).

References

1. Polack FP, Thomas SJ, Kitchin N, Absalon J, Gurtman A, Lockhart S, et al. Safety and Efficacy of the BNT162b2 mRNA Covid-19 Vaccine. N Engl J Med. 2020;383(27):2603–15.
2. Baden LR, El Sahly HM, Essink B, Kotloff K, Frey S, Novak R, et al. Efficacy and Safety of the mRNA-1273 SARS-CoV-2 Vaccine. N Engl J Med. 2021;384(5):403–16.
3. Voysey M, Clemens SAC, Madhi SA, Weckx LY, Folegatti PM, Aley PK, et al. Safety and efficacy of the ChAdOx1 nCoV-19 vaccine (AZD1222) against SARS-CoV-2: an interim analysis of four randomised controlled trials in Brazil, South Africa, and the UK. Lancet. 2021;397(10269):99–111.
4. Wang P, Liu L, Iketani S, Luo Y, Guo Y, Wang M, et al. Increased Resistance of SARS-CoV-2 Variants B.1.351 and B.1.1.7 to Antibody Neutralization. bioRxiv. 2021 Jan 1;2021.01.25.428137.
5. Zhang W, Davis BD, Chen SS, Martinez JMS, Plummer JT, Vail E. Emergence of a novel SARS-CoV-2 strain in Southern California, USA. medRxiv. 2021 Jan 1;2021.01.18.21249786.
6. Yuan M, Wu NC, Zhu X, Lee C-CD, So RTY, Lv H, et al. A highly conserved cryptic epitope in the receptor binding domains of SARS-CoV-2 and SARS-CoV. Science (80-). 2020 May 8;368(6491):630 LP – 633.
7. Rogers TF, Zhao F, Huang D, Beutler N, Burns A, He W, et al. Isolation of potent SARS-CoV-2 neutralizing antibodies and protection from disease in a small animal model. Science (80-). 2020 Aug 21;369(6506):956 LP – 963.
8. Banach BB, Cerutti G, Fahad AS, Shen C-H, Olivera de Souza M, Katsamba PS, et al. Paired Heavy and Light Chain Signatures Contribute to Potent SARS-CoV-2 Neutralization in Public Antibody Responses. SSRN Electron J. 2021.
9. Wrapp D, Wang N, Corbett KS, Goldsmith JA, Hsieh C-L, Abiona O, et al. Cryo-EM structure of the 2019-nCoV spike in the prefusion conformation. Science (80-). 2020 Mar 13;367(6483):1260 LP – 1263.
10. Starr TN, Greaney AJ, Hilton SK, Crawford KHD, Jane M, Bowen JE, et al. Deep mutational scanning of SARS-CoV-2 receptor binding domain reveals constraints on folding and ACE2 binding. 2020;1–40.
11. Greaney AJ, Starr TN, Gilchuk P, Zost SJ, Binshtein E, Loes AN, et al. Complete Mapping of Mutations to the SARS-CoV-2 Spike Receptor-Binding Domain that Escape Antibody Recognition. Cell Host Microbe . 2020;29(1):44-57.e9.
12. Pinto D, Park Y-J, Beltramello M, Walls AC, Tortorici MA, Bianchi S, et al. Cross-neutralization of SARS-CoV-2 by a human monoclonal SARS-CoV antibody. Nature. 2020 Jul;583(7815):290–5.
13. Tan CW, Chia WN, Qin X, Liu P, Chen MI-C, Tiu C, et al. A SARS-CoV-2 surrogate virus neutralization test based on antibody-mediated blockage of ACE2-spike protein-protein interaction. Nat Biotechnol. 2020 Sep;38(9):1073–8.
14. Wrenbeck EE, Klesmith JR, Stapleton JA, Adeniran A, Tyo KEJ, Whitehead TA. Plasmid-based one-pot saturation mutagenesis. Nat Methods. 2016;13(11):928–30.
15. An enrichment ratio for a specific mutant is the log2 transform of the frequency of the mutant in the sorted population relative to the same mutant in the reference population.
16. Wu Y, Wang F, Shen C, Peng W, Li D, Zhao C, et al. A noncompeting pair of human

neutralizing antibodies block COVID-19 virus binding to its receptor ACE2. Science (80-). 2020 Jun 12;368(6496):1274 LP – 1278.
17. Wu NC, Yuan M, Liu H, Sanders RW, Ward AB, Wilson IA, et al.An Alternative Binding Mode of IGHV3-53 Antibodies to the SARS-CoV-2 Receptor Binding Domain. CellReports. 2020;33(3):108274.
18. Yuan M, Liu H, Wu NC, Lee C-CD, Zhu X, Zhao F, et al. Structural basis of a shared antibody response to SARS-CoV-2. Science (80-). 2020 Aug 28;369(6507):1119 LP – 1123.
19. Weisblum Y, Schmidt F, Zhang F, Dasilva J, Poston D, Lorenzi JCC, et al. Escape from neutralizing antibodies by SARS-CoV-2 spike protein variants. 2020;1–31.
20. Liu Z, VanBlargan LA, Bloyet LM, Rothlauf PW, Chen RE, Stumpf S, et al. Identification of SARS-CoV-2 spike mutations that attenuate monoclonal and serum antibody neutralization. Cell Host Microbe. 2021;1–12.
21. Baum A, Fulton BO, Wloga E, Copin R, Pascal KE, Russo V, et al. Antibody cocktail to SARS-CoV-2 spike protein prevents rapid mutational escape seen with individual antibodies. Science (80-). 2020;0831(June):eabd0831.
22. Li Q, Wu J, Nie J, Li Q, Wu J, Nie J, et al. The Impact of Mutations in SARS-CoV-2 Spike on Viral Infectivity and Antigenicity. Cell. 2020;182(5):1284-1294.e9.
23. Barnes CO, Jette CA, Abernathy ME, Dam KA, Esswein SR, Gristick HB, et al. SARS-CoV-2 neutralizing antibody structures inform therapeutic strategies. Nature. 2020;588(August).
24. Chi X, Yan R, Zhang J, Zhang G, Zhang Y, Hao M, et al. A neutralizing human antibody binds to the N-terminal domain of the Spike protein of SARS-CoV-2. Science (80-). 2020 Aug 7;369(6504):650 LP – 655.
25. Humphrey W, Dalke A, Schulten K. VMD: Visual molecular dynamics. J Mol Graph. 1996;14(1):33–8.

Figures

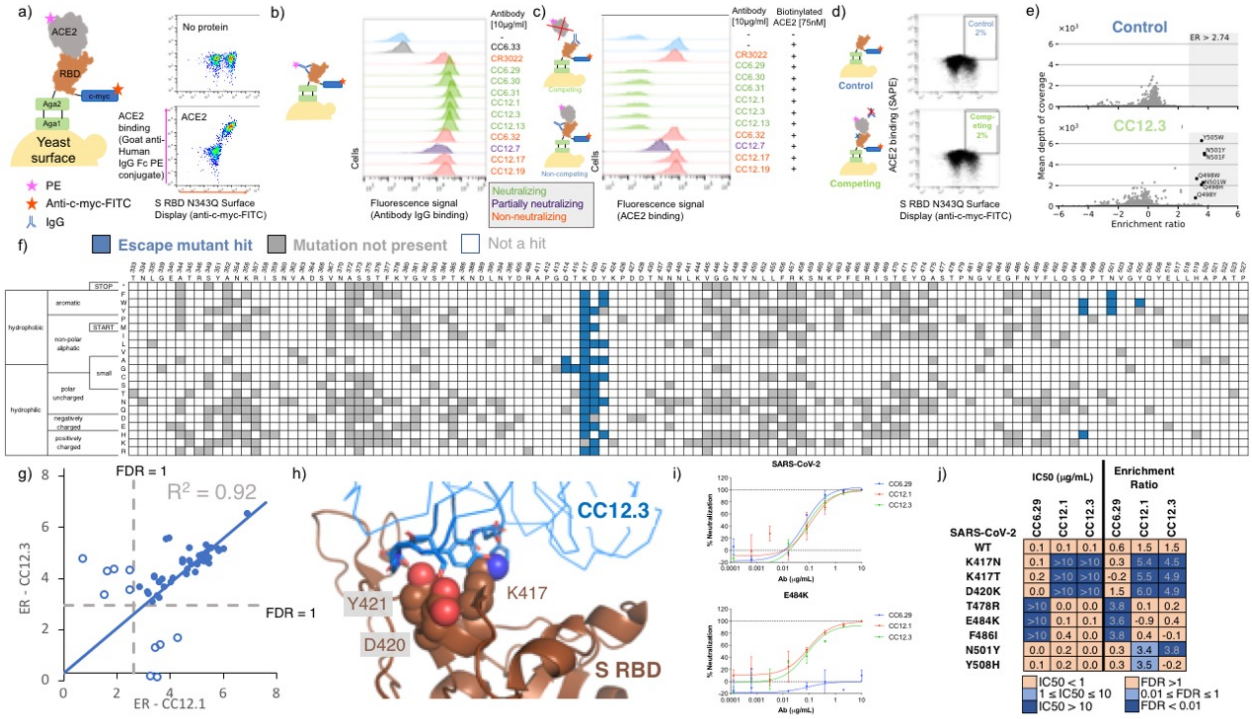

Figure 1. Identification and validation of SARS-CoV-2 S RBD escape mutants using yeast screening. **a)** Cartoon of the yeast display construct S-RBD(333-537)-N343Q. Cytograms show specific binding in the presence, but not absence, of ACE2-Fc. **b)** Binding profiles of aglycosylated S RBD labeled with 10 μg/mL of indicated mAb. Antibodies are color coded according to neutralization potency *(7)*. **c.)** Competitive binding between IgG and ACE2 was performed by labeled yeast displaying aglycosylated S RBD with 10 μg/mL of indicated mAbs followed by labeling with biotinylated ACE2. **d.)** Single site saturation mutagenesis S RBD libraries were sorted by FACS using a competition experiment. The top cytogram shows the cell population collected for the control population without ACE2 labeling, while the bottom cytogram shows the cell population enriched in mutations able to bind ACE2 in the presence of a competing IgG. The specific cytogram shown is for nAb CC12.3 using the S RBD library corresponding to mutations at positions 437-537. **e.)** Per-mutation enrichment ratio distributions as a function of average depth of coverage control (top) and CC12.3 nAb competing experiment (bottom). **f.)** Heatmap showing predicted S RBD escape mutants for CC12.3 in blue. White cells are mutations with a p value for an FDR > 1, while grey cells are mutations not present in the mutational library. S RBD positions directly involved in binding ACE2 are colored gray. **g.)** Comparison of enrichment ratios (ER) for individual hits for CC12.3 vs. CC12.1. Closed circles represent escape mutant hits for both nAbs, whereas open circlers are escape mutant hits for only one nAb. **h.)** Solved structure of nAB CC12.3 in complex with S RBD (PDB ID 7KN6). **i.)** PSV neutralization curves for CC12.1, CC12.3 and CC6.29 on SARS-CoV-2 (top) and SARS-CoV-2 E484K (bottom). **j.)** PSV IC50 analysis for CC12.1, CC12.3 and CC6.29 on different identified mutations.

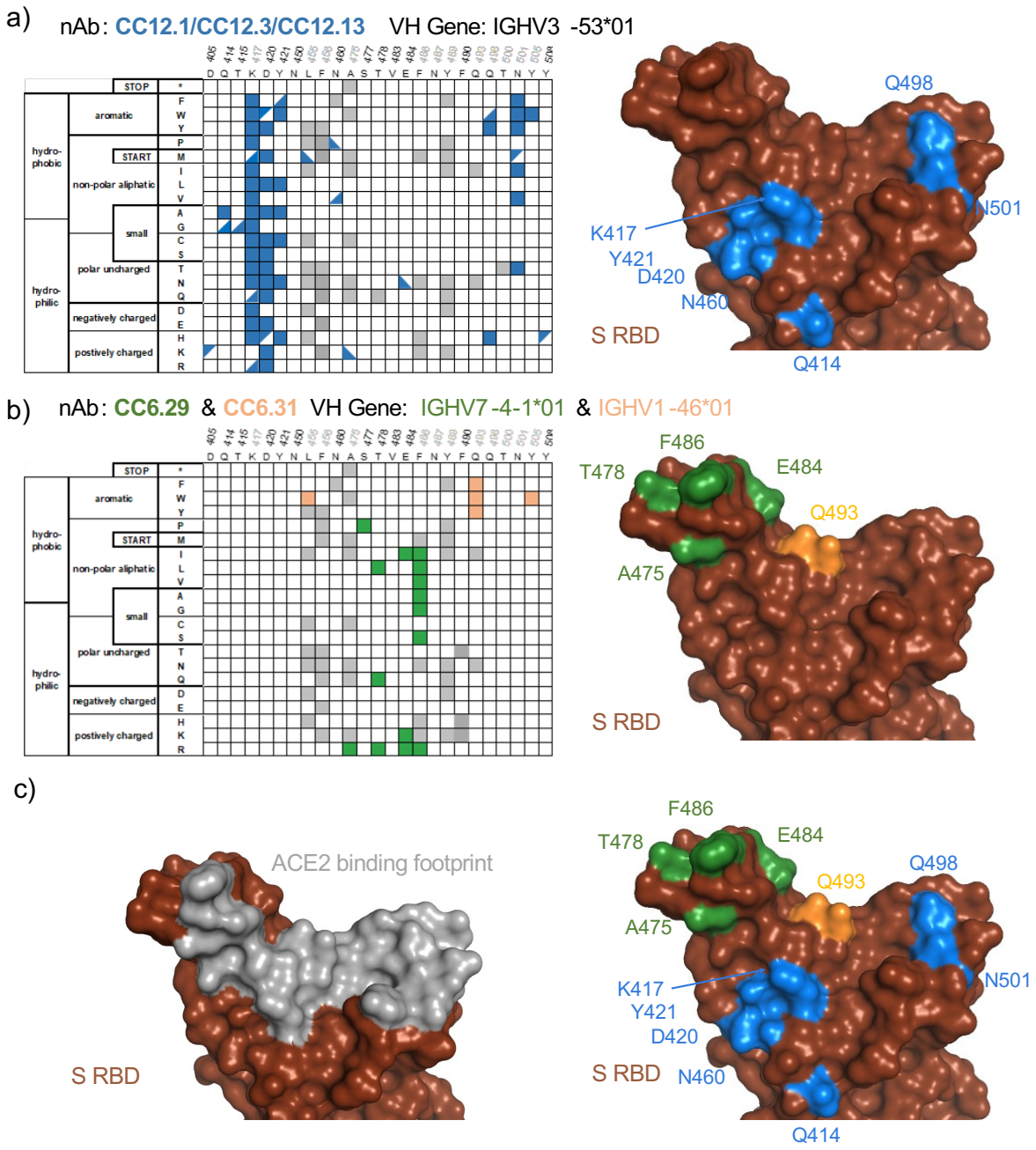

Figure 2. Sequence determinants and structural basis of S RBD escape mutants. a-c) (left) Limited per-position heatmap and (right) mutations mapped onto the S RBD-ACE2 structural complex (PDB ID: 6M0J). For clarity, only positions with two or more escape mutations are shown with surface colored. Panels are for **a)** nAbs CC12.1, CC12.3, and CC12.13. Boxes indicate escape mutants for two or more nAbs, while triangles indicate an escape mutant identified for just one nAb (top left: CC12.1, bottom right: CC12.3, bottom left: CC12.13) ; **b)** CC6.29 and CC6.31 (orange); **c)** overlay of escape mutants from all nAbs onto the S RBD-ACE2 structural complex.

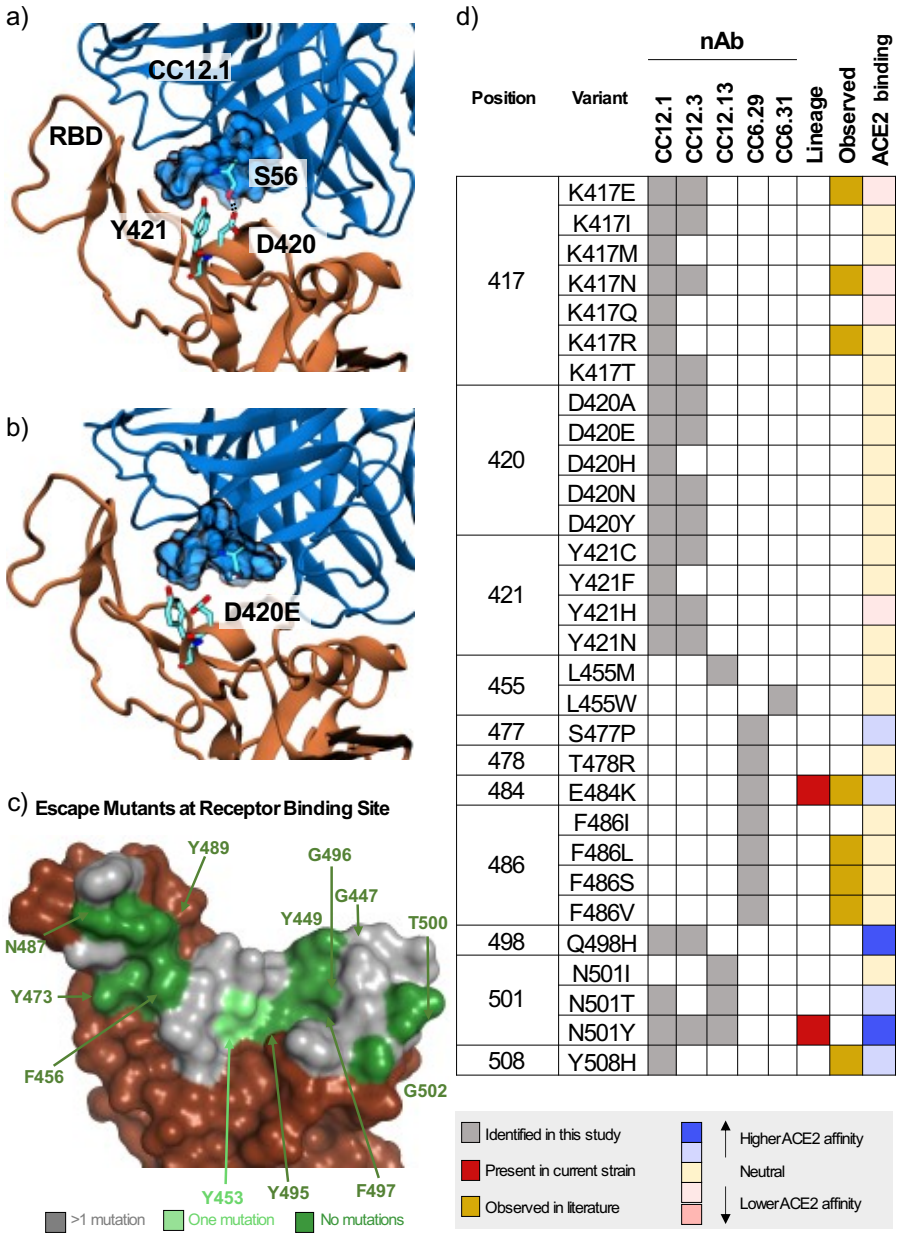

Figure 3. Mechanistic, structural, and sequence analysis of SARS-CoV-2 escape mutants. **a-b)** Snapshots from MD trajectories showing **a.)** key interactions in the control simulation of S RBD in complex with CC12.1, and **b.)** mechanism of escape of S RBD from CC12.1 due to the D420E mutation. Images were rendered with Visual Molecular Dynamics (VMD *(25)*), and black dotted lines indicate persistent hydrogen bonds. **c.)** S RBS positions are colored by the number of escape mutants identified to date. RBS residues involving the S RBD-ACE2 structural complex (PDB ID: 6M0J) are colored by number of escape mutants identified to date. **d.)** Summary of 1-nt escape mutants identified in the present study. Lineage column indicates presence of the given mutation amongst currently circulating SARS-CoV-2 strains, while the observed column refers to an escape mutant previously identified in literature *(11, 19–22)*. ACE2 binding indicates affinity to ACE2 based on the measurements by Starr et al. *(10)*.

Supplementary Materials for

One-shot identification of SARS-CoV-2 S RBD escape mutants using yeast screening

Irene Francino Urdaniz[1,#], Paul J. Steiner[1,#], Monica B. Kirby[1,#], Fangzhu Zhao[2], Cyrus M. Haas[1], Shawn Barman[2], Emily R. Rhodes[1], Linghang Peng[2], Kayla G. Sprenger[1], Joseph G. Jardine[2,3], Timothy A. Whitehead[1,*]

[1]Department of Chemical and Biological Engineering, University of Colorado, Boulder, CO 80305, USA
[2]The Scripps Research Institute, La Jolla, CA, USA
[3]International AIDS Vaccine Initiative, New York, NY, USA

# Co-authors contributed equally.
*Correspondence to: timothy.whitehead@colorado.edu

This PDF file includes:

Materials and Methods
Figures S1 to S17
Tables S1 to S5
Captions for Data S1 to S3

Other Supplementary Materials for this manuscript include the following:

Data S1 to S3

Materials and Methods

Plasmid constructs

All plasmids used for this work are listed in **Table S4** and all primers in **Table S5**. All plasmids were verified by Sanger sequencing. Yeast display constructs for SARS-CoV-2 spike protein ectodomain (GenBank MN908947 with a GSAS substitution at the furin cleavage site (682-685) and proline substitutions at positions 986 and 987 (1), and a C-terminal T4 fibritin trimerization domain), as shown in **Figure S1**, were constructed as follows. Spike was codon optimized for *Saccharomyces cerevisiae* with Benchling software using default options, split into three gene blocks (hereafter labeled A, B, and C) each encoded with BsaI restriction sites with overhangs (2), synthesized as gBlocks (IDT), and cloned into pUC19 (Addgene: #50005) using SalI/KpnI restriction sites. This yielded the spike fragment entry plasmids pUC19-S-ecto-B and pUC19-S-ecto-C-Nterm. To construct pUC19-S-ecto-A-Nterm-KanR (the spike fragment destination plasmid), PCR was used to amplify both the kanamycin resistance gene from pETconNK (Addgene: #81169) with primers MBK-175 and MBK-176, and the pUC19-S-ecto-A-Nterm plasmid with primers MBK-177 and MBK-178. NEBuilder HiFi DNA Assembly protocol (NEB) was used to insert the kanamycin resistance gene into the plasmid. pUC19-S-ecto-Nterm was constructed by Golden Gate cloning (3) using pUC19-S-ecto-A-Nterm-KanR, pUC19-S-ecto-B, and pUC19-S-ecto-C-Nterm.

To construct pJS698 (N-terminal fusion **Spike ectodomain** YSD backbone), pETconNK-Nterm-Aga2p was first constructed by inserted a gene block with a multiple cloning site between the AGA2 signal peptide and the remainder of the AGA2 coding sequence following standard restriction enzyme cloning practices. pETconNK-Nterm-Aga2p was amplified with primers PJS-P2194 and PJS-P2195 using KAPA HiFi HotStart Readymix (Kapa Biosystems). The reaction was fractionated by agarose gel electrophoresis and the 6062 bp band excised and purified using a Monarch DNA Gel Extraction kit (NEB). The fragment (40 ng) was circularized using the Q5® Site-Directed Mutagenesis Kit (NEB) in a 10 µl reaction and transformed into E. coli Mach1 chemically competent cells (Invitrogen).

To construct pJS697 (C-terminal fusion **RBD** YSD backbone), pETconNK (Addgene: #81169) was amplified with primers PJS-P2192 and PJS-P2193 using KAPA HiFi HotStart Readymix (Kapa Biosystems). The reaction was fractionated by agarose gel electrophoresis and the 6084 bp band excised and purifed using a Monarch DNA Gel Extraction kit (NEB). The fragment (40 ng) was circularized using the Q5® Site-Directed Mutagenesis Kit (NEB) in a 10 µl reaction and transformed into *E. coli* Mach1 chemically competent cells (Invitrogen).

pJS699 (S-RBD(333-537)-N343Q for fusion to the C-terminus of AGA2) was previously described (4).

Recombinant protein production, purification, and preparation

ACE2-Fc was produced and purified following Walls et al. 2020 (5). CR3022 (6) was expressed by transient transfection in Expi293F cells and purified by protein A affinity chromatography and SEC using a Superdex 200 10/300 GL. Specificity was verified by measuring binding to SARS-CoV-2 RBD and irrelevant antigen. The anti-SARS-CoV-2 RBD antibody panel used (CC6.29, CC6.31, CC6.32, CC6.33, CC12.1, CC12.3, CC12.7, CC12.13, CC12.17, CC12.19) was a kind

gift from Dennis Burton's lab at Scripps and were produced and purified according to Rogers et al. (7).

All proteins that were chemically biotinylated were prepared at a 20:1 molar ratio of biotin to protein using EZ-Link NHS-Biotin (Thermo Scientific) according to manufacturer's protocol. All proteins were stored at 4 °C in phosphate buffered saline (8 g/L NaCl, 0.2 g/L KCl, 1.44g/L Na_2HPO_4, 0.24g/L KH_2PO_4) pH 7.4.

Preparation of Mutagenic Libraries

All 119 surface exposed residues on S RBD (positions 333-537) were mutated to every other amino acid plus stop codon using NNK primers (**Table S5**) using comprehensive nicking mutagenesis exactly as described (8). For compatibility with Illumina sequencing, two tiles were made: tile 1 encompassed residues 333-436, while tile 2 encompassed residues 437-527 containing the critical receptor binding site. Serial dilutions were plated to calculate the transformation efficiency (**Table S1**). Glycerol stocks were made for each tile.

To create the display construct of S-RBD(333-537)-N343Q fused to the C-terminus of Aga2p, pJS697 was digested with BsaI-HFv2 (NEB) and purified using a Monarch PCR & DNA Cleanup Kit (NEB). Each mutated pJS699 library was digested with NotI-HF (NEB), the reaction fractionated by agarose gel electrophoresis, and the band corresponding to S-RBD (0.83kb) excised and purified using a Monarch DNA Gel Extraction Kit (NEB). Yeast transformation was performed exactly as described (9). For each library, the two fragments were co-transformed (in a 3:1 molar ratio of S-RBD to backbone) into chemically competent *S. cerevisiae* EBY100 (10). Serial dilutions were plated on SDCAA and incubated 3 days to calculate the efficiency of the transformation (**Table S1**). Biological replicates were made on a different day by co-transforming each tile into EBY100 exactly as described. Yeast stocks for each transformation were stored in yeast storage buffer at -80°C.

Mutagenic libraries for the N-terminal spike orientation were constructed following oligo pool mutagenesis exactly as described (8,11) using pUC19-S-ecto-A-Nterm-KanR, pUC19-S-ecto-B, and pUC19-S-ecto-C-Nterm as templates. For the oligo pool we computationally selected 1,909 mutations hypothesized to either destabilize the 'down' conformation, stabilize the 'up' conformation, or both (**Data S2**). The majority of these mutations targeted S_1 (94%, 1793/1909) at the NTD, RBD, SD1, and SD2 domains, with the remainder mapping to the boundary between the HR1 and CH domains on S_2. After mutagenesis, the mutational libraries were digested with BsaI-HFv2, fractionated by agarose gel electrophoresis, and gel excised and purified with Monarch Gel Extraction kit (NEB). 40 fmol of pUC19-S-ecto-A-NSM-Nterm-KanR, pUC19-S-ecto-B-NSM, and pUC19-S-ecto-C-NSM-Nterm were ligated together with T4 DNA Ligase (NEB), cleaned up and concentrated each to a final volume of 6µl with Monarch PCR & DNA Cleanup kit (NEB), and transformed into chemically competent *E.coli* Mach1 cells (Invitrogen cat. #C862003). The resulting library had on average 3 mutations per spike protein per plasmid. Library statistics were determined post sequencing.

To construct the surface display library in yeast, the spike plasmid library was digested with NotI-HF (NEB) and the S coding region was gel purified. The YSD vector pJS698 was digested with BsaI-HFv2 and column purified. 1.3 µg of insert (S coding region) and 1.7 µg of vector were

electroporated into 400 µl EBY100 using the method of Benatuil et al. (12) as written, except that electroporation was performed at 2 kV rather than 2.5 kV. Immediately after electroporation, serial dilutions were plated on SDCAA Agar to calculate the complexity of the library. After electroporation, the cells were immediately transferred to 50 ml SDCAA (20g/L dextrose, 6.7g/L Difco yeast nitrogen base, 5g/L Bacto casamino acids, 5.4g/L Na_2HPO_4, and 8.56g/L $NaH_2PO_4 \cdot H_2O$) and grown at 30 ºC for two days to saturation. The cultures were passaged twice in medium M37D (diluted to OD_{600} = 0.05 in 120 ml, then to OD_{600} = 0.4 in 50 ml) and stocks prepared at OD_{600} = 1 as in Whitehead et al. (13). The final composition of M37 is 20 g L^{-1} **d**extrose or **g**alactose (for M37D, M37G respectively), 5 g L^{-1} casamino acids, 6.7 g L^{-1} yeast nitrogen base with ammonium sulfate, 50 mM citric acid, 50 mM phosphoric acid, 80 mM MES acid, neutralized with 90% sodium hydroxide / 10% potassium hydroxide to pH 7. Both media should be prepared by dissolving all reagents except yeast nitrogen base into MilliQ water, adjusting the pH to 7.0 with freshly prepared sodium hydroxide / potassium hydroxide mixture, and adjusting the volume to $9/10^{th}$ of the final desired volume. Pass the solution through a 0.22 µm filter, both for sterility and to remove particulates that would nucleate struvite. Finish the media by addition of $1/10^{th}$ volume of 10x filtered yeast nitrogen base.

Yeast Display Titrations and Competition Binding

For cell surface titrations, EBY100 harboring the RBD display plasmid was grown in 1 ml M19D (5 g/l casamino acids, 40 g/l dextrose, 80 mM MES free acid, 50 mM citric acid, 50 mM phosphoric acid, 6.7 g/l yeast nitrogen base, adjusted to pH7 with 9M NaOH, 1M KOH) overnight at 30°C. Expression was induced by resuspending the M19D culture to OD_{600}=1 in M19G (5 g/l casamino acids, 40 g/l galactose, 80 mM MES free acid, 50 mM citric acid, 50 mM phosphoric acid, 6.7 g/l yeast nitrogen base, adjusted to pH7 with 9M NaOH, 1M KOH) and growing 22 h at 22°C with shaking at 300 rpm. For CR3022 IgG, yeast surface display titrations were performed as described by Chao et al. (14) with an incubation time of 4h at room temperature and using secondary labels anti-c-myc-FITC (Miltenyi Biotec) and Goat anti-Human IgG Fc PE conjugate (Invitrogen Catalog # 12-4998-82). Titrations were performed in biological replicates and technical triplicates (n = 6). The levels of display and binding were assessed by fluorescence measurements for FITC and SAPE using the Sony SH800 cell sorter equipped with a 70µm sorting chip and 488nm laser.

To test the individual antibody panel binding to S RBD, EBY100 harboring the RBD display plasmid was grown from -80ºC cell stocks in 1 ml SDCAA for 4h at 30ºC. Expression was induced by resuspending the SDCAA culture to OD_{600}=1 in SGCAA and growing at 22h at 22°C with shaking at 300rpm. $1x10^5$ yeast cells were labelled with 10 μg/ml antibody IgG for 30min at room temperature in PBSF (PBS containing 1g/l BSA). The cells were centrifuged and washed with 200 µL PBSF. They were labeled with 0.6 µL FITC (Miltenyi Biotec), 0.25 µL Goat anti-Human IgG Fc PE (ThermoFisher Scientific) and 49.15 µL PBSF for 10min at 4°C. Cells were then centrifuged, washed with PBSF, and read on a flow cytometer to measure binding of the ACE2. Experiments were performed at least in biological replicate.

Competitive binding assays on the yeast surface were performed between a free antibody and biotinylated ACE2. *S. cerevisiae* EBY100 harboring the RBD display plasmid was grown from -80ºC cell stocks in 1 ml SDCAA for 4h at 30ºC. Expression was induced by resuspending the SDCAA culture to OD_{600}=1 in SGCAA and growing at 22h at 22°C with shaking at 300rpm. $1x10^5$ yeast cells were labelled with 10 μg/ml antibody IgG for 30min at room temperature in PBSF (PBS

containing 1g/l BSA). The same cells were labelled with 30nM chemically biotinylated hACE2, in the same tube without washing, for 30min at room temperature in PBSF. The cells were centrifuged and washed with 200 μL PBSF. They were labeled with 0.6 µL FITC (Miltenyi Biotec), 0.25 µL SAPE (Invitrogen) and 49.15 µL PBSF for 10min at 4°C. Cells were then centrifuged, washed with PBSF. The pellet was resuspended in 100 μL and read on a flow cytometer to measure binding of the hACE2.

Yeast Display Screening of S and S RBD libraries

For full-length S ectodomain screening, pUC19-S-ecto-Nterm and pJS698 were independently linearized via digest with restriction enzymes at 37°C for 1 hour, and gel extracted based off size using Monarch DNA Gel Extraction Kit. The linearized regions were co-transformed in a molar ratio of 1:3 insert to vector into chemically competent EBY100 following published protocols (9). EBY100 cells were recovered in nuclease free water for 5 minutes and then plated on two different yeast media agar plates: SDCAA and M37D. Cells were incubated at 30°C for 3 days. After initial growth, colonies from each plate were selected and grown up at 30°C and 250rpm overnight in the respective dextrose media: SDCAA, M37D. Cells were then induced in respective galactose media at an OD_{600}=1 at three different temperatures, 18°C, 22°C, and 30°C for 20 hours.

Induced EBY100 cells were washed with PBSF (8 g/L NaCl, 0.2 g/L KCl, 1.44g/L Na_2HPO_4, 0.24g/L KH_2PO_4, and 1g/L bovine serum albumin, pH to 7.4 and filter sterilized) and resuspended in PBSF at an OD_{600}=10. The cells were then incubated with either 500nM of the biotinylated ACE2-Fc or 500nM of the biotinylated CR3022 for 1 hour at room temperature. The cells were then washed with PBSF and labeled with anti-cmyc fluorescein isothiocyanate (FITC) (Miltenyi Biotec) and streptavidin phycoerythrin (SAPE) (Invitrogen) and incubated on ice for 10 minutes.

The Spike mutagenic library was labeled with CR3022 and, separately, ACE2-Fc under the optimal conditions were screened. Approximately 10^8 were sorted using fluorescence activated cell sorting (FACS), and the top 1% of cells by fluorescence were collected. The two resulting sorted libraries were expanded and sorted in a second round, again screening 10^8 cells and collecting the top 1% by fluorescence intensity. The selected populations were amplified and purified based on tile, deep sequenced, and count data compared with a reference population.

For the escape mutant screening of the S RBD, $3x10^7$ induced EBY100 yeast cells displaying S RBD were labelled with 10 μg/ml antibody IgG for 30min at room temperature with mixing by pipetting every 10min in PBSF (PBS containing 1g/l BSA). The same cells were labelled with 75nM chemically biotinylated ACE2, in the same tube, for 30min at room temperature in PBSF with mixing by pipetting every 10min. The cells were centrifuged and washed with 1mL PBSF. Cells were then labeled with 1.2 µL FITC, 0.5 µL SAPE and 98.3 µL PBSF for 10min at 4°C. Cells were centrifuged, washed with 1mL PBSF, resuspended to 1 mL PBSF and sorted using FACS. Multiple gates were used for sorting as shown in **Figure S6**, including an FSC/SSC^+ gate for isolation of yeast cells, FSC-H/FSC-A gate to discriminate single cells, and the top 2% by a $PE^+/FITC^+$ gate. At least $3.0x10^5$ cells were collected and were recovered in SDCAA with 50 μg/mL Kanamycin and 1x PenStrep for 30h. Biological replicates were sorted as described except for the ACE2 concentration being 30nM, maintaining saturation conditions.

Deep Sequencing Preparation

Libraries were prepared for deep sequencing following the "Method B" protocol from Kowalsky et al (15) exactly as described for the spike ectodomain libraries and with a few changes for the RBD libraries. A Monarch PCR & DNA Cleanup kit was used. PCR of extracted and cleaned-up yeast plasmid DNA was performed using 2xQ5 HotStart Master Mix (NEB) and the following protocol:

- 1 min @ 98 °C
- 25 cycles of:
    - 10 sec @ 98 °C
    - 20 sec @ 64 °C
    - 30 sec (replicate 1) or 1 min (replicate 2) @ 72 °C
- 2 min @ 72 °C
- Hold @ 4 °C

Primers used in library prep are given in **Table S5**. Amplicons were fractionated by agarose gel electrophoresis and purified using a Monarch DNA Gel Extraction Kit (NEB). Samples were then further purified using Agencourt Ampure XP beads (Beckman Coulter), quantified using PicoGreen (ThermoFisher), pooled, and sequenced on an Illumina MiSeq using 2 x 250 bp paired-end reads at the BioFrontiers Sequencing Core (University of Colorado, Boulder, CO).

Deep Sequencing Analysis

All deep sequencing data analysis was performed by scripts written in Python, available at GITHUB (https://github.com/WhiteheadGroup/SpikeRBDStabilization.git).

Because all sequenced samples were PCR amplicons of known length, paired-end reads were merged by aligning at the known overlap. Mismatches in overlapping regions were resolved by selecting the base pair with the higher quality score and assigning it a quality score given by the absolute difference of the quality scores at the mismatch. Paired reads with more than 10 mismatches in the overlapping region and merged reads containing any quality score less than 10 were discarded. The total number of retained reads in each sample was recorded as n_i, the number of reads in sample i.

Each read was compared to the wild-type sequence to identify all mutations. Counts for synonymous single mutations were combined to give k_{ij}, the number of reads in sample i encoding the single amino acid mutation j. Reads including multiple mutations or mutations not encoded in the library oligos were not analyzed further. The frequency of single mutant j in sample i was calculated as $f_{ij} = k_{ij} \,/\, n_i$.

Each experiment consisted of two samples: a reference sample r and a selected sample s. For each experiment, the risk ratio of variant j was calculated as $\rho_j = f_{sj} \,/\, f_{rj}$ i.e. the ratio of the variant's frequency in the selected population to its frequency in the reference population. Enrichment ratios were calculated as the binary logarithm of the risk ratio: $ER_j = \rho_j$. Variants with five or fewer counts in the reference population were not analyzed further. Variants with at least five counts in the reference population but no counts in the selected population were given a pseudocount of one.

Determining hits from yeast display screens

For each escape mutant screen, we collected the top 2% (PE channel) of the population of $FITC^+$ (RBD displaying) cells. This population was not labeled with biotinylated ACE2 and so serves as a null experiment where the observed enrichment ratios are due to other sources of variance and not to differential nAb binding. We fit the distribution of enrichment ratios for each of these control samples using kernel density estimation (KDE) (SciPy's scipy.stats.gaussian_kde with default parameters) (16). We then treated this distribution estimate as an empirical null hypothesis. Under this null hypothesis, we expect $N\left(1 - F(ER_t)\right)$ false positives, where N is the number of variants tested, F is the cumulative distribution function (CDF) of the control ER KDE, and ER_t is a threshold. Therefore, for a target false discovery rate (FDR), we chose $ER_t = F^{-1}(1 - FDR/N)$, where F^{-1} is the inverse CDF of the KDE. In data from samples labeled with nAbs, we then tested the hypothesis that each observed ER was greater than the associated ER_t using an one-sided exact Poisson rate ratio test (statsmodels.stats.rates.test_poisson_2indep from the Python library statsmodels) (17). For these tests, the null ratio was 2^{ER_t}. The counts were given by the number of reads for the variant in the selected and reference populations, respectively, and the exposures were given by the total number of reads in the reference and selected populations, respectively. For this analysis, we identified hits for replicate 1 (tiles 1 & 2 for nAbs CC6.29, CC12.1, and CC12.3) using a target FDR of 1 and a Poisson rate ratio test significance level of 0.01. For replicate 2 (tile 2 for nAbs CC6.31, CC12.13) escape mutant hits were identified using a target FDR of 1.

For the full-length S ectodomain screen, our null experiment was the collected reference populations without selections for each of the ACE2-Fc and CR3022 experiments. These reference populations were passaged, sorted, and amplified identically to the sorted libraries except that no screen was employed. We fit the distribution of enrichment ratios for these control samples using a logistic CDF (custom MATLAB script), and the empirical FDR was calculated exactly as above.

Molecular Dynamics Simulations

GROMACS 2018.3 (25) was employed for all molecular dynamics (MD) simulations along with the TIP3P (26) water model and Amber99SB-ILDN (27) force field to model the receptor binding domain (RBD) of the spike (S) protein of SARS-CoV-2 and neutralizing antibodies CC12.1 and CC12.3. Simulations were initiated from crystal structures of the RBD in complex with CC12.1 (PDB code 6XC2 (28)) and CC12.3 (PDB code 6XC4 (28)). All systems containing a positive charge were neutralized by the addition of Cl- ions, also modeled with the Amber99SB-ILDN force field. Each simulation consisted of approximately 192,000 atoms.

A steepest descent energy minimization of the initial coordinates for each system was carried out for 5,000 steps. NVT equilibration simulations were then performed for 0.5 ns at 310 K with the Bussi−Donadio−Parrinello (29) thermostat. Subsequent NPT equilibration simulations were performed for 1 ns at 310 K and 1.0 bar, using the same thermostat and Berendsen (30) barostat. The time constant for coupling in both the NVT and NPT simulations was 0.1 ps. Production simulations in the NPT ensemble were then carried out at 310 K and 1.0 bar with the Bussi−Donadio−Parrinello thermostat and Parrinello–Rahman (31) barostat. Long-range electrostatic interactions were calculated using particle mesh Ewald summations and a cutoff of 1.0 nm, and Lennard Jones interactions were calculated over 1.0 nm and shifted beyond this distance. Neighbor lists were updated every 10 steps with a cutoff of 1.0 nm. Bonds between hydrogen and heavy atoms were constrained with the LINCS (32) algorithm. Furthermore, periodic boundary conditions were used in all simulations in all directions. Production simulations

were carried out for 100 ns, leading to a total of 0.8 microseconds of simulation time across the eight simulations.

Pseudo Neutralization Assays

SARS-CoV-2 pseudovirus neutralization assays were performed as previously described (7). Briefly, pseudovirus was generated by cotransfecting MLV-gag/pol and MLV-CMV-Luciferase plasmids with truncated wildtype SARS-CoV-2 or mutant SARS-CoV-2 plasmid respectively onto HEK293T cells. After 48h or 72h of transfection, supernatants containing pseudovirus were collected and frozen at -80 °C. Neutralization assay was performed as follows. First, monoclonal antibodies were serially diluted into half-area 96-well plates (Corning, 3688) and incubated with pseudovirus at 37 °C for 1 h. Next, HeLa-hACE2 cells were transferred in the 96-well plates at 10,000 cells/well. After 48h of incubation, supernatants were removed, cells were lysed with 1x luciferase lysis buffer (25 mM Gly-Gly pH 7.8, 15 mM MgSO4, 4 mM EGTA, 1% Triton X-100). Finally, Bright-Glo (Promega, PR-E2620) was added onto 96-well plates according to manufacturer's instructions. Neutralization IC50s were calculated using "One-Site LogIC50" regression in GraphPad Prism 8.0. Pseudovirus mutant constructs were generated by amplifying two overlapped fragments of SARS-CoV-2 mutant sequences with Q5 enzyme (NEB, M0492) following manufacturer's instructions. Two fragments were then joint into one fragment by bridge PCR, and gibson cloned into digested pcDNA3.3 backbone.

References

1. Wrapp D, Wang N, Corbett KS, Goldsmith JA, Hsieh C-L, Abiona O, et al. Cryo-EM structure of the 2019-nCoV spike in the prefusion conformation. Science (80-) [Internet]. 2020 Mar 13;367(6483):1260 LP – 1263. Available from: http://science.sciencemag.org/content/367/6483/1260.abstract
2. Potapov V, Ong JL, Kucera RB, Langhorst BW, Bilotti K, Pryor JM, et al. Comprehensive Profiling of Four Base Overhang Ligation Fidelity by T4 DNA Ligase and Application to DNA Assembly. ACS Synth Biol. 2018;7(11):2665–74.
3. Engler C, Marillonnet S. Golden Gate Cloning. In: Valla S, Lale R, editors. DNA Cloning and Assembly Methods [Internet]. Totowa, NJ: Humana Press; 2014. p. 119–31. Available from: https://doi.org/10.1007/978-1-62703-764-8_9
4. Banach BB, Cerutti G, Fahad AS, Shen C-H, Olivera de Souza M, Katsamba PS, et al. Paired Heavy and Light Chain Signatures Contribute to Potent SARS-CoV-2 Neutralization in Public Antibody Responses. SSRN Electron J. 2021;
5. Walls AC, Park Y-J, Tortorici MA, Wall A, McGuire AT, Veesler D. Structure, Function, and Antigenicity of the SARS-CoV-2 Spike Glycoprotein. Cell [Internet]. 2020;1–12. Available from: http://www.ncbi.nlm.nih.gov/pubmed/32155444
6. ter Meulen J, van den Brink EN, Poon LLM, Marissen WE, Leung CSW, Cox F, et al. Human Monoclonal Antibody Combination against SARS Coronavirus: Synergy and Coverage of Escape Mutants. PLOS Med [Internet]. 2006;3(7). Available from: https://doi.org/10.1371/journal.pmed.0030237
7. Rogers TF, Zhao F, Huang D, Beutler N, Burns A, He W, et al. Isolation of potent SARS-CoV-2 neutralizing antibodies and protection from disease in a small animal model. Science (80-) [Internet]. 2020 Aug 21;369(6506):956 LP – 963. Available from: http://science.sciencemag.org/content/369/6506/956.abstract
8. Wrenbeck EE, Klesmith JR, Stapleton JA, Adeniran A, Tyo KEJ, Whitehead TA. Plasmid-based one-pot saturation mutagenesis. Nat Methods [Internet]. 2016;13(11):928–30. Available from: https://doi.org/10.1038/nmeth.4029
9. Medina-Cucurella A V., Whitehead TA. Characterizing protein-protein interactions using deep sequencing coupled to yeast surface display. In: Methods in Molecular Biology. 2018.
10. Boder ET, Wittrup KD. Yeast surface display for screening combinatorial polypeptide libraries. Nat Biotechnol [Internet]. 1997;15(6):553–7. Available from: https://doi.org/10.1038/nbt0697-553
11. Medina-Cucurella A V., Steiner PJ, Faber MS, Beltrán J, Borelli AN, Kirby MB, et al. User-defined single pot mutagenesis using unamplified oligo pools. Protein Eng Des Sel. 2019;32(1):41–5.
12. Benatuil L, Perez JM, Belk J, Hsieh CM. An improved yeast transformation method for the generation of very large human antibody libraries. Protein Eng Des Sel. 2010;23(4):155–9.
13. Whitehead TA, Chevalier A, Song Y, Dreyfus C, Fleishman SJ, De Mattos C, et al. Optimization of affinity, specificity and function of designed influenza inhibitors using deep sequencing. Nat Biotechnol. 2012 May;30(6):543–8.
14. Chao G, Lau WL, Hackel BJ, Sazinsky SL, Lippow SM, Wittrup KD. Isolating and engineering human antibodies using yeast surface display. Nat Protoc. 2006;1(2):755–68.

15. Kowalsky CA, Klesmith JR, Stapleton JA, Kelly V, Reichkitzer N, Whitehead TA. High-resolution sequence-function mapping of full-length proteins. PLoS One. 2015;10(3):1–23.
16. Shalloo RJ, Dann SJD, Gruse J-N, Underwood CID, Antoine AF, Arran C, et al. Automation and control of laser wakefield accelerators using Bayesian optimization. Nat Commun [Internet]. 2020;11(1):6355. Available from: https://doi.org/10.1038/s41467-020-20245-6
17. Seabold S, Perktold J. Statsmodels : Econometric and Statistical Modeling with Python. Proc 9th Python Sci Conf. 2010;Vol. 57(Scipy):92–6.
18. Yuan M, Wu NC, Zhu X, Lee CCD, So RTY, Lv H, et al. A highly conserved cryptic epitope in the receptor binding domains of SARS-CoV-2 and SARS-CoV. Science (80-). 2020;368(6491):630–3.
19. Liu Z, VanBlargan LA, Bloyet LM, Rothlauf PW, Chen RE, Stumpf S, et al. Identification of SARS-CoV-2 spike mutations that attenuate monoclonal and serum antibody neutralization. Cell Host Microbe [Internet]. 2021;1–12. Available from: https://doi.org/10.1016/j.chom.2021.01.014
20. Weisblum Y, Schmidt F, Zhang F, Dasilva J, Poston D, Lorenzi JCC, et al. Escape from neutralizing antibodies by SARS-CoV-2 spike protein variants. 2020;1–31.
21. Greaney AJ, Starr TN, Gilchuk P, Zost SJ, Binshtein E, Loes AN, et al. Complete Mapping of Mutations to the SARS-CoV-2 Spike Receptor-Binding Domain that Escape Antibody Recognition. Cell Host Microbe [Internet]. 2020;29(1):44-57.e9. Available from: https://doi.org/10.1016/j.chom.2020.11.007
22. Baum A, Fulton BO, Wloga E, Copin R, Pascal KE, Russo V, et al. Antibody cocktail to SARS-CoV-2 spike protein prevents rapid mutational escape seen with individual antibodies. Science [Internet]. 2020;0831(May):1–8. Available from: http://www.ncbi.nlm.nih.gov/pubmed/32540904
23. Li Q, Wu J, Nie J, Li Q, Wu J, Nie J, et al. Article The Impact of Mutations in SARS-CoV-2 Spike on Viral Infectivity and Antigenicity ll ll Article The Impact of Mutations in SARS-CoV-2 Spike on Viral Infectivity and Antigenicity. Cell [Internet]. 2020;182(5):1284-1294.e9. Available from: http://dx.doi.org/10.1016/j.cell.2020.07.012
24. Lee ME, DeLoache WC, Cervantes B, Dueber JE. A Highly Characterized Yeast Toolkit for Modular, Multipart Assembly. ACS Synth Biol. 2015 Sep;4(9):975–86.
25. Abraham, M. J. *et al.* GROMACS: High performance molecular simulations through multi-level parallelism from laptops to supercomputers. *SoftwareX* **1**–**2**, 19–25 (2015).
26. Jorgensen, W. L., Chandrasekhar, J., Madura, J. D., Impey, R. W. & Klein, M. L. Comparison of simple potential functions for simulating liquid water. *J. Chem. Phys.* **79**, 926–935 (1983).
27. Lindorff-Larsen, K. *et al.* Improved side-chain torsion potentials for the Amber ff99SB protein force field. *Proteins Struct. Funct. Bioinforma.* (2010) doi:10.1002/prot.22711.
28. Yuan, M. *et al.* Structural basis of a shared antibody response to SARS-CoV-2. *Science (80-.).* (2020) doi:10.1126/science.abd2321.
29. Bussi, G., Donadio, D. & Parrinello, M. Canonical sampling through velocity rescaling. *J. Chem. Phys.* **126**, 014101 (2007).
30. Berendsen, H. J. C., Postma, J. P. M., van Gunsteren, W. F., DiNola, A. & Haak, J. R. Molecular dynamics with coupling to an external bath. *J. Chem. Phys.* **81**, 3684–3690 (1984).

31. Parrinello, M. & Rahman, A. Polymorphic transitions in single crystals: A new molecular dynamics method. *J. Appl. Phys.* **52**, 7182–7190 (1981).
32. Hess, B., Bekker, H., Berendsen, H. J. C. & Fraaije, J. G. E. M. LINCS: A linear constraint solver for molecular simulations. *J. Comput. Chem.* **18**, 1463–1472 (1997).
33. Kumari, R., Kumar, R. & Lynn, A. G-mmpbsa -A GROMACS tool for high-throughput MM-PBSA calculations. *J. Chem. Inf. Model.* (2014) doi:10.1021/ci500020m.
34. Baker, N. A., Sept, D., Joseph, S., Holst, M. J. & McCammon, J. A. Electrostatics of nanosystems: Application to microtubules and the ribosome. *Proc. Natl. Acad. Sci. U. S. A.* **98**, 10037–10041 (2001).

FIGURES

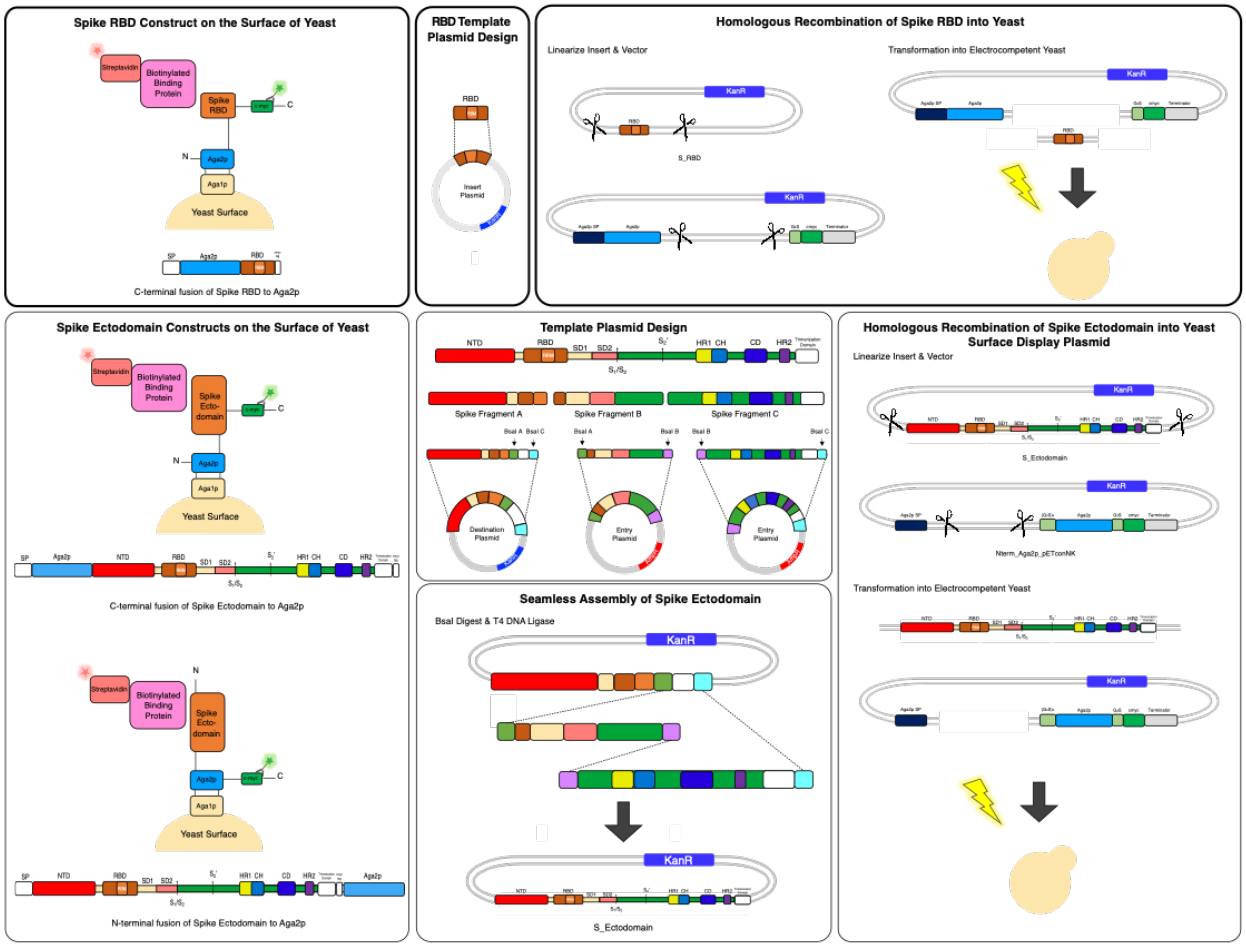

Fig. S1. Overview of yeast display constructs used in screening S RBD and prefusion stabilized S ectodomain libraries.

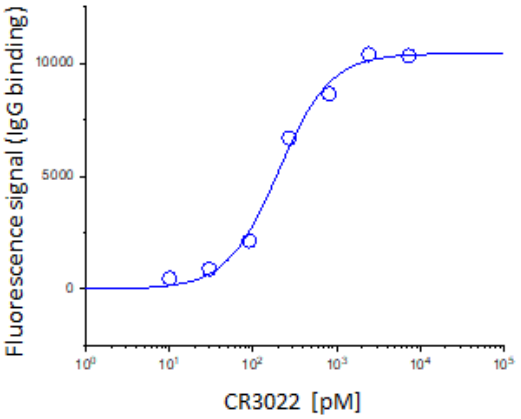

IgG	Apparent K_d, YSD [pM]	Apparent K_d, *in vitro* [pM]	Reference
CR3022	171±25	~ 100	Yuan, et al. 2020
910-30	230±70	104	Banach, et al. 2021

Fig. S2. Non-neutralizing antibody CR3022 dissociation constant compared to literature. Yeast cell surface titrations of non neutralizing CR3022 IgG against aglycosylated S RBD yield an apparent K_D of 171 ± 25 pM. Technical triplicates were performed (n = 3), and error reported is 2 s.e.m. Data for the HKU 910-30 nAb is from Banach et al, 2021. (4,18).

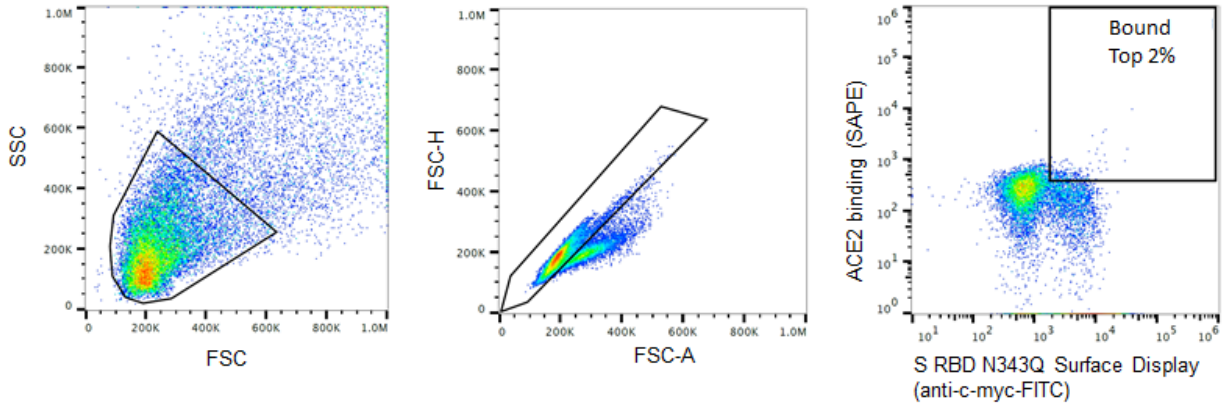

Fig. S3. FACS sorting gates used to collect S RBD escape mutants
Representative sorting gates used for all escape mutant FACS screens. The three gates were SSC/FSC; FSC-H/FSC-A to discriminate single yeast cells; and $SAPE^{+}/FITC^{+}$ to identify mutants that allow ACE2 binding in the presence of 10 μg/mL antibody. Shown here are gates for the antibody CC6.29.

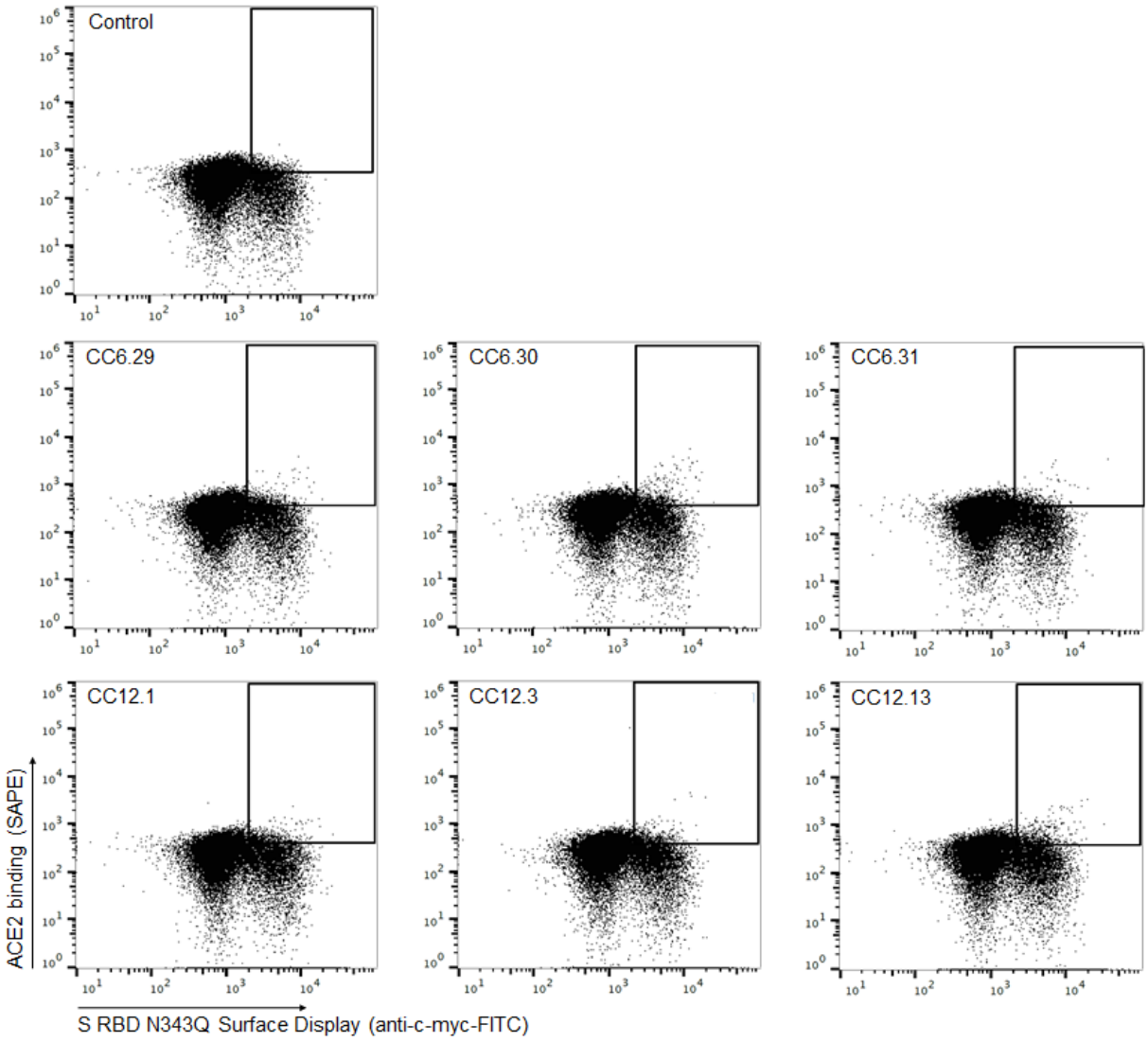

Fig. S4. Sorting gates for competitive binding experiments.
PE/FITC cytograms for aglycosylated S RBD yeast libraries sorted using competitive binding with ACE2-Fc. The top cytogram shows the control experiment with no ACE2 labeling. Gates represent the top 2% of the $FITC^{+}$ cells by PE signal for each antibody used in the study.

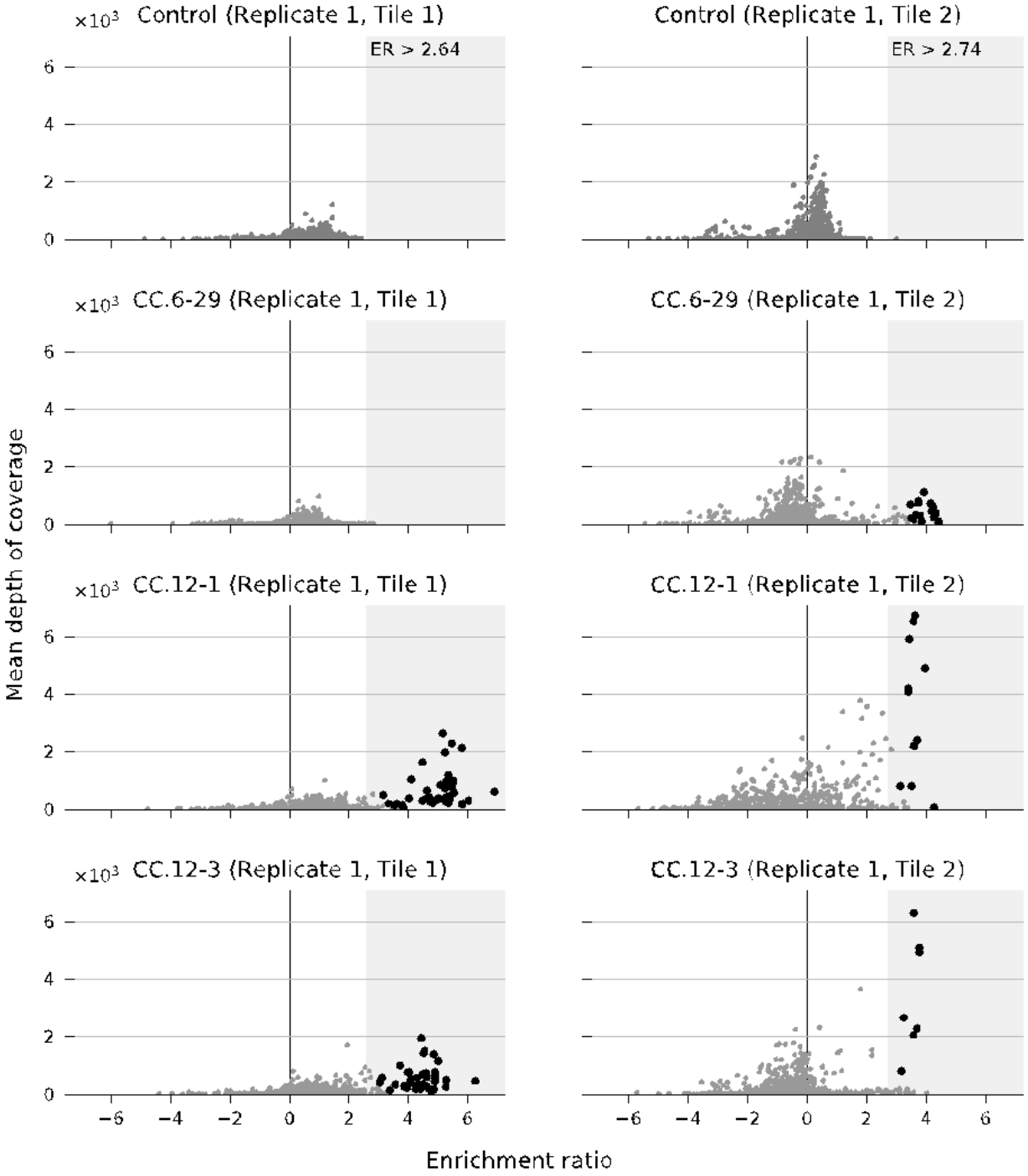

Fig. S5. Per-mutation enrichment ratio (ER) distributions as a function of average depth of coverage control (top) and CC12.3, CC12.1, CC6.29 nAb competing experiment (bottom). ER thresholds determined for FDR = 1 are shown in the control panels (top). Hits (with ER greater than the threshold at p <= 0.01) are shown with larger black dots.

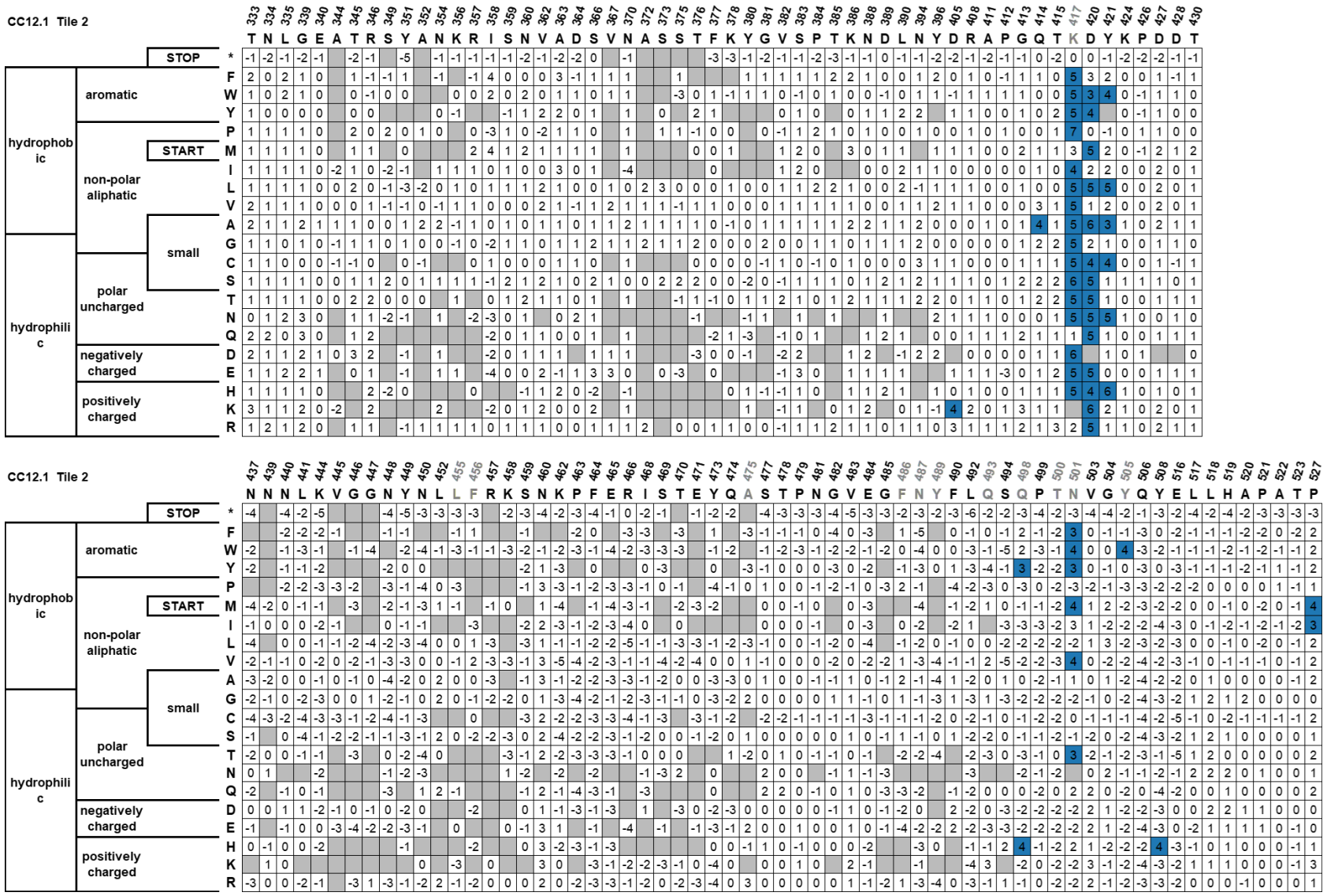

Fig. S6. CC12.1 heatmap using FDR < 0.1 as cut-off. Blue - escape mutant hit, white – not a hit, grey – mutation not present. Position numbers in grey indicate ACE2 footprint.

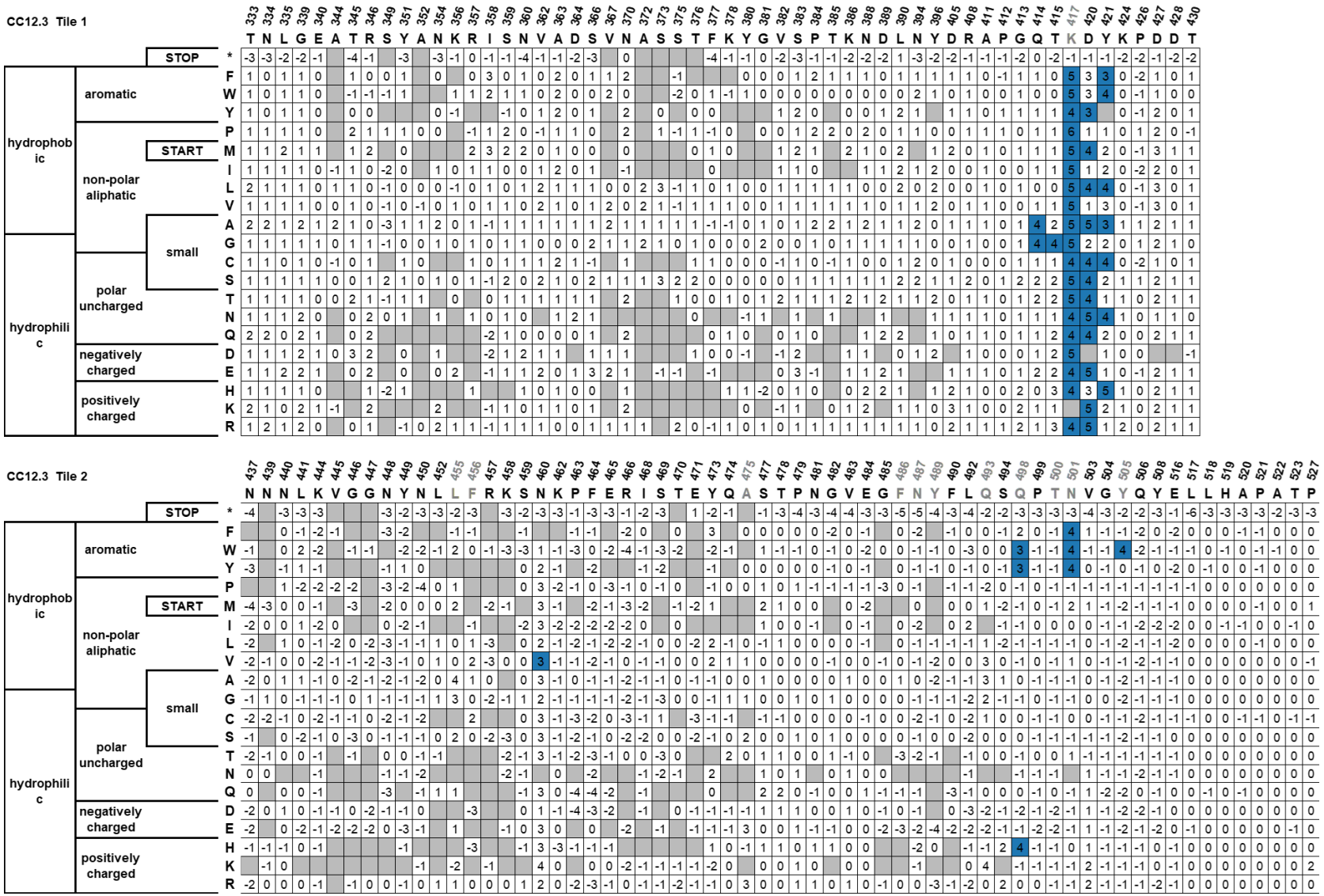

Fig. S7. CC12.3 heatmap using FDR < 0.1 as cut-off. Blue - escape mutant hit, white – not a hit, grey – mutation not present. Position numbers in grey indicate ACE2 footprint.

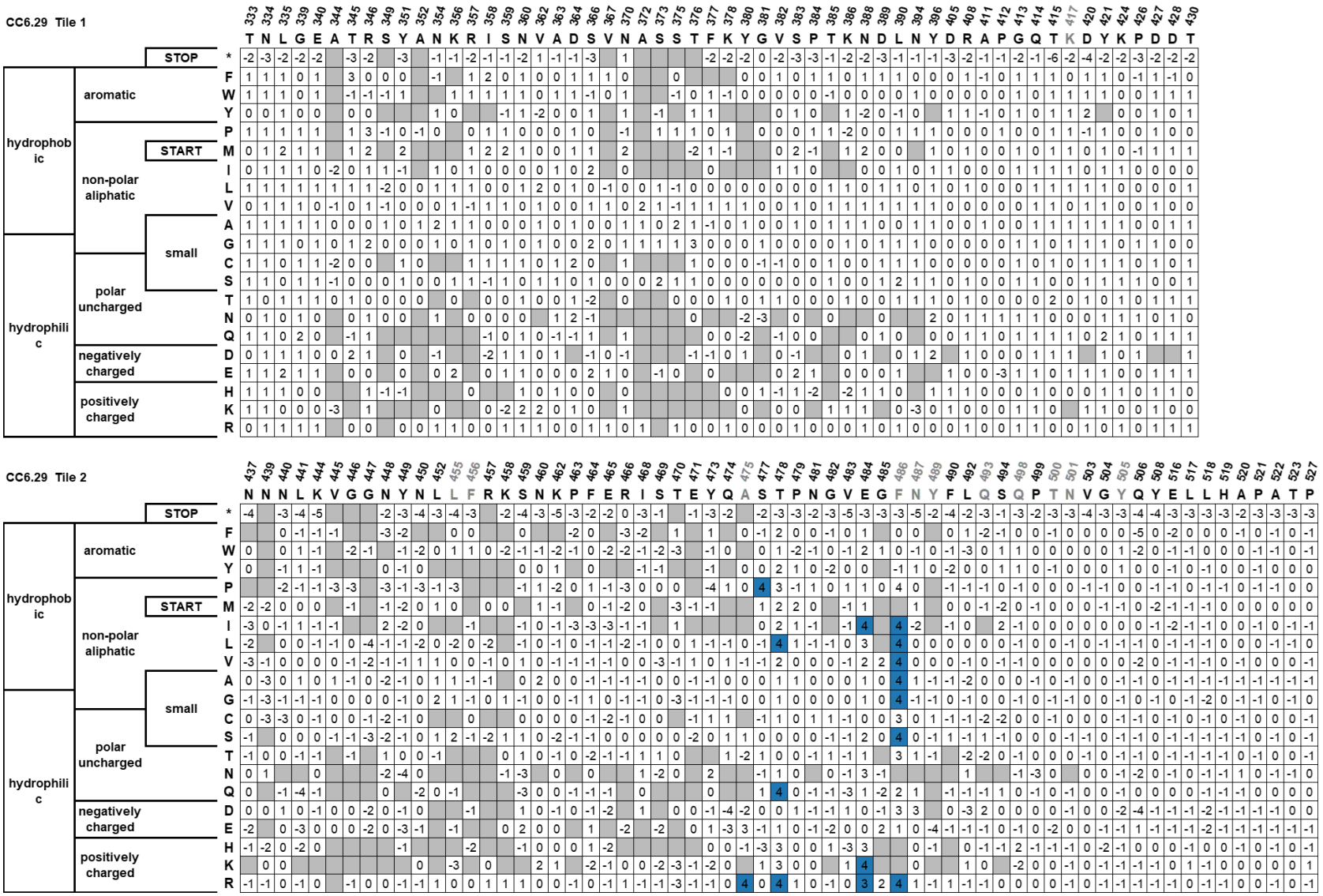

Fig. S8. CC6.29 heatmap using FDR < 0.1 as cut-off. Blue - escape mutant hit, white – not a hit, grey – mutation not present. Position numbers in grey indicate ACE2 footprint.

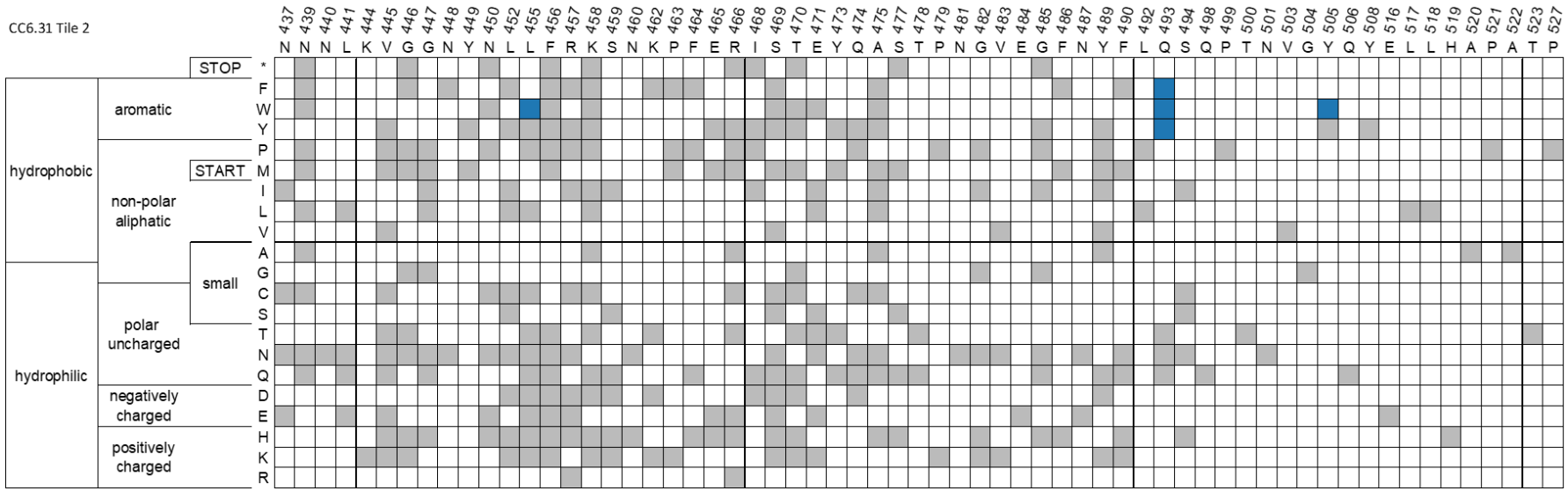

Fig. S9. CC6.31 heatmap using FDR < 1 as cut-off. Blue - escape mutant hit, white – not a hit, grey – mutation not present. Position numbers in grey indicate ACE2 footprint.

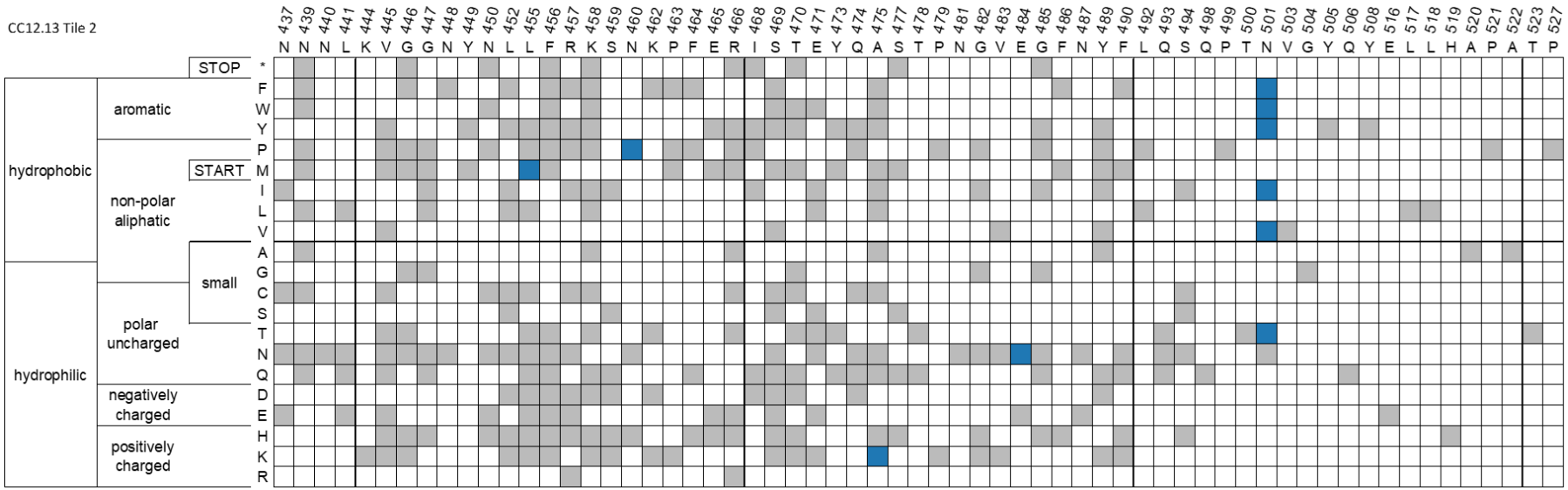

Fig. S10. CC12.13 heatmap using FDR < 1 as cut-off. Blue - escape mutant hit, white – not a hit, grey – mutation not present. Position numbers in grey indicate ACE2 footprint.

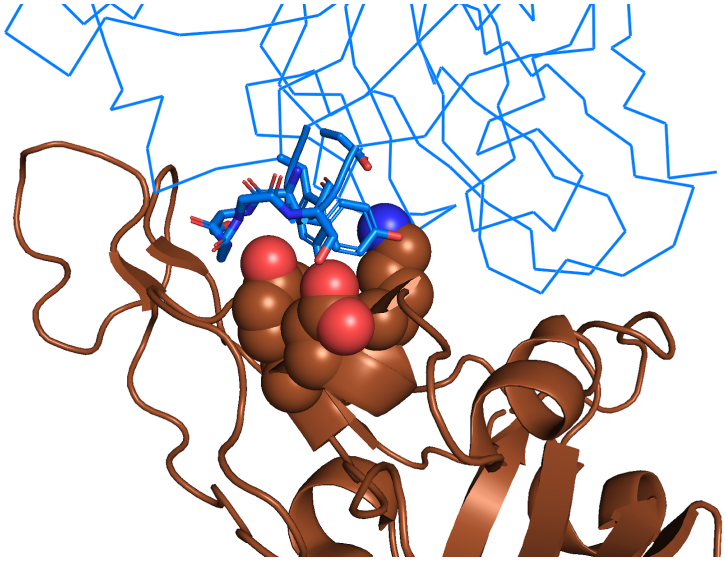

Fig. S11. Structural recognition of S RBD (chocolate cartoon) by nAB CC12.1 (PDB ID 6XC2, blue ribbon). S positions K417, D420, Y421 are shown as spheres and the CDR H2 and key CC12.1 residues are shown as sticks.

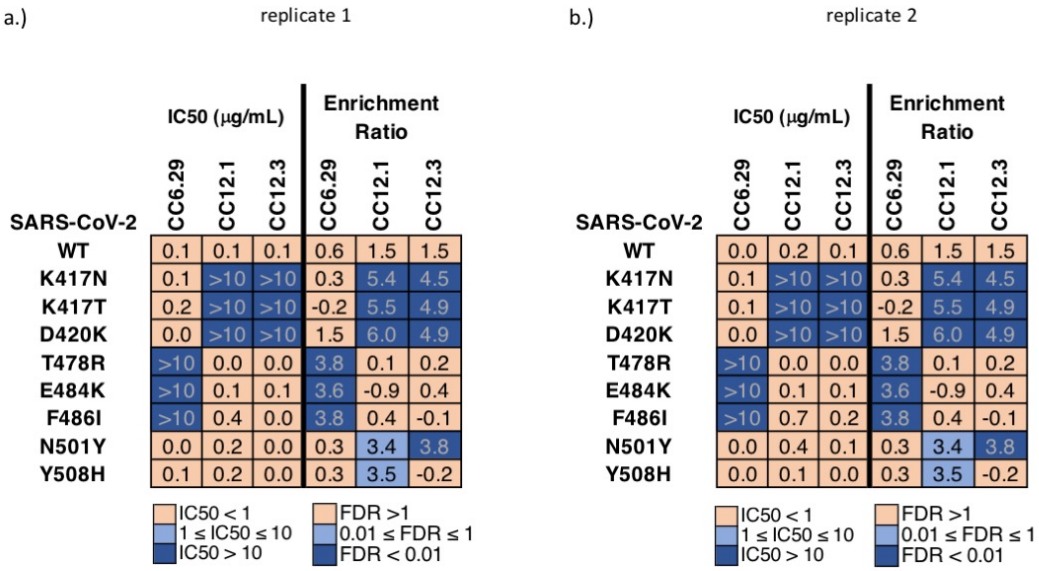

Fig. S12. MLV-based SARS-CoV-2 pseudovirus neutralization assays for SARS-CoV-2 RBD variants. Data shown are replicates of the neutralization assays repeated on separate days (replicate 1 - day 1; replicate 2 - day 2). IC50 neutralization values shown are averages of two technical replicates. Replicate 1 data is also presented in Figure 1j of the main text.

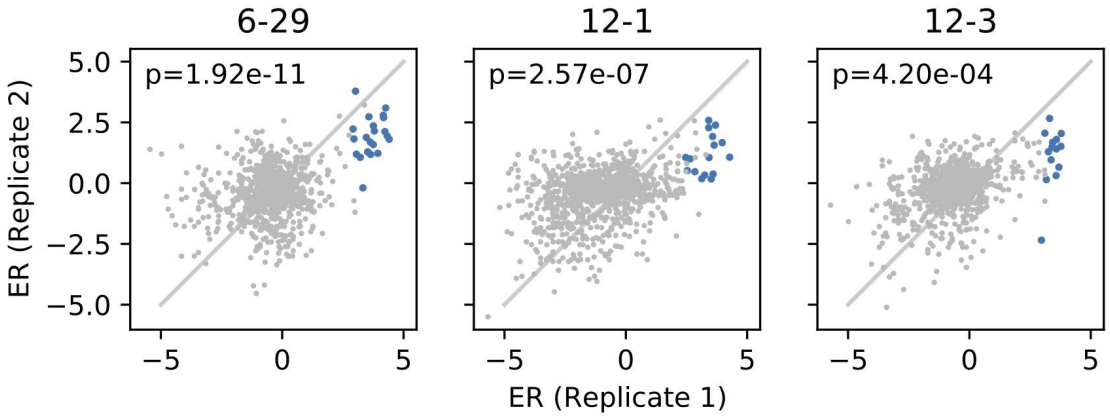

Fig. S13. Comparison between biological replicates for S RBD positions 437-527 for CC6.29, CC12.1, and CC12.3. Escape mutant hits identified in replicate 1 are shown as closed blue circles (a p <= 0.01 for an FDR < 1). p-values are calculated using a one-sided Welch's t-test with the alternative hypothesis that the mean enrichment ratio from the replicate 2 hits are > the mean enrichment ratio from the replicate 2 non-hits.

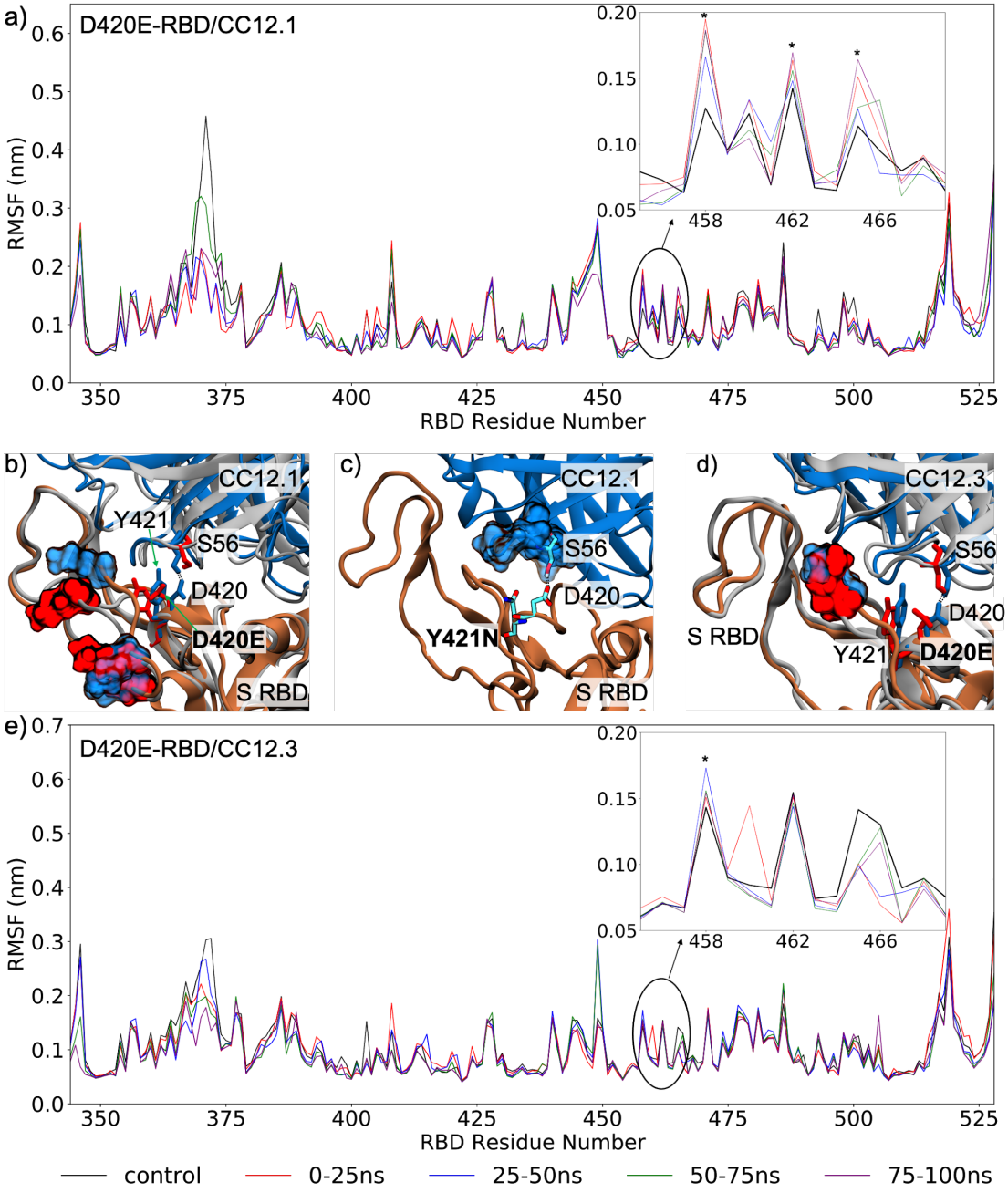

Fig. S14. (a) Comparison of the root mean square fluctuation (RMSF) profile of CC12.1 in complex with wildtype/control S RBD (averaged across the 100 ns production run) and S RBD with the D420E mutation (averaged across 25 ns intervals). (b) Structural mapping of highly fluctuating residues on S RBD with the D420E mutation, identified in panel (a), when complexed with CC12.1. Wildtype and mutant RBDs are shown in brown and gray and CC12.1 in blue and gray, respectively, while residues are colored blue for wildtype RBD and red for the mutant RBD; highly fluctuating residues are shown in surface representation. (c) MD snapshot showing the proposed mechanism of escape of S RBD from CC12.1 through mutation Y421N. (d) Structural mapping of highly fluctuating residues on S RBD with the D420E mutation, identified in panel (e), when complexed with CC12.3. (e) Comparison of the RMSF profile of CC12.3 in complex with wildtype S RBD and S RBD with the D420E mutation.

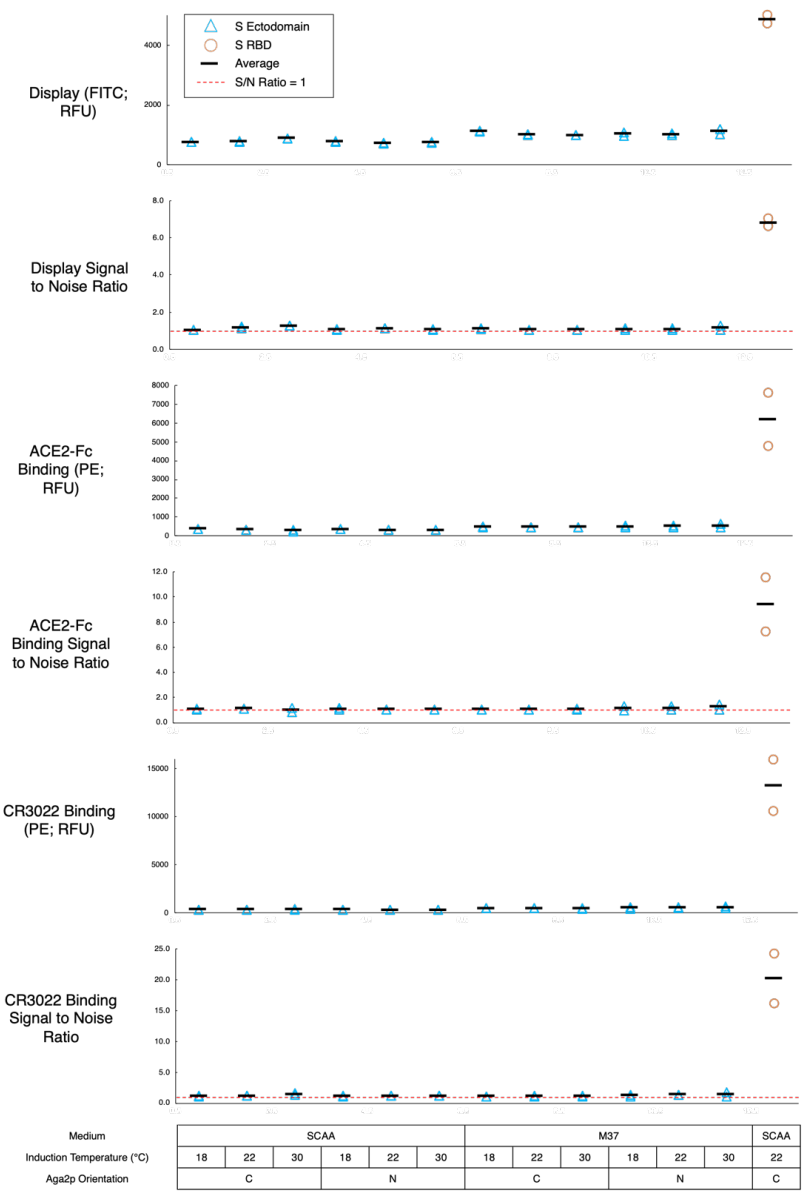

Fig. S15: Yeast surface display for SARS-CoV-2 prefusion stabilized S ectodomain compared to S RBD. FITC signal (RFU), FITC signal to noise ratio, and PE signal (RFU) and PE signal to noise ratio for both ACE2-Fc and CR3022 are shown for biological replicates of spike ectodomain with differing media, induction temperatures, and orientation of Spike relative to Aga2p (blue triangles). The FITC fluorescence derives from an anti-cmyc FITC antibody that recognizes a C-terminal cmyc epitope tag for displayed protein, while the PE signal is from biotinylated ACE2-Fc or CR3022 subsequently labeled with streptavidin-PE. The concentration of the secondary binding protein for the S ectodomain was 500nM ACE2-Fc and 500nM CR3022. FITC signal (RFU), FITC signal to noise ratio, and PE signal (RFU) and PE signal to noise ratio for both ACE2-Fc and CR3022 shown for S RBD at optimal conditions (orange circles). The concentration of secondary binding protein for the S RBD is at 1 nM, which is at saturation.

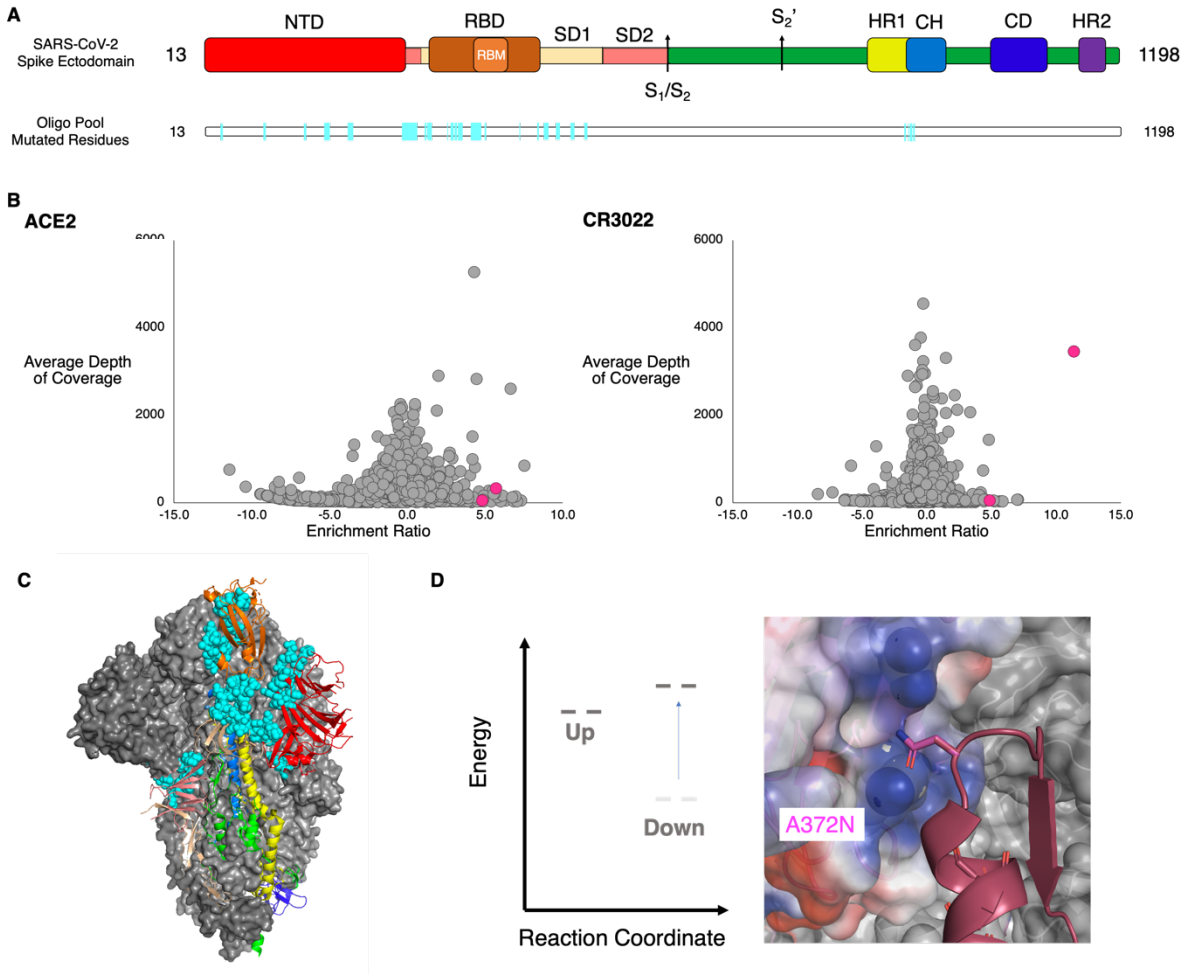

Fig. S16. Determination and location of potential stabilizing hits. (A) Spike ectodomain schematic with labeled and colored boundaries. Below schematic is the locations of the mutated residues in the oligo pool, cyan, as well as locations of the top identified hits shown in magenta. NTD: N-terminal domain, RBD: receptor-binding domain, RBM: receptor-binding motif, SD1: subdomain 1, SD2: subdomain 2, S_1/S_2: furin cleavage site, S_2': S_2' cleavage site, HR1: heptad repeat 1, CH: central helix, CD: connector domain, HR2: heptad repeat 2. (B) Average depth of coverage vs. Enrichment ratio for single mutants for (left) ACE2 and (right) CR3022. All mutations are shown in gray with the two hits (K113I & A372N) colored magenta. (C) Prefusion spike trimer shown with domains colored as they are in panel A. RBD is shown in the up conformation and along with SD1 and SD2 is shown on the same spike monomer. The NTD and S2 subunits are shown on a neighboring monomer. Oligo pool mutated residues are represented as cyan spheres. (D) Putative reaction coordinate and interaction of hit A372N in the spike ectodomain. A372N is hypothesized to destabilize the down protomer by steric repulsion with an adjacent 'down' protomer.

TABLES

Table S1.

Summary of Statistics for S RBD & N-Term Spike ectodomain Libraries. Library statistics for S RBD were determined by tabulating all variants with at least two reads in the yeast reference libraries. Library statistics for S ectodomain were determined from NGS of the libraries harbored in *E. coli*.

	S RBD		**S Ecto**				
Tile Number	Tile 1	Tile 2	Tile 1	Tile 2	Tile 3	Tile 4	Tile 5
Positions	333-436	437-537	31-177	189-341	355-494	510-589	936-1020
Number of Designed Mutations	1120	1260	229	582	639	324	135
Transformants Obtained from Nicking Saturation Mutagenesis	1.10E+06	2.70E+07		2.00E+06		1.00E+06	1.00E+04
Transformants Obtained from Assembly of Spike Ectodomain	N/A				4.00E+05		
Transformants Obtained from Homologous Recombination	2.50E+05	1.10E+05			1.75E+06		
Library Coverage Per Tile	97% (1085/1120)	94% (1189/1260)	88% (201/229)	90% (523/582)	90% (577/639)	100% (324/324)	99% (134/135)
Overall Library Coverage	96% (2274/2380)		92% (1759/1909)				

Table S2. List of escape mutants identified in this study. Escape mutants were identified by a p value < 0.01 for containing a FDR < 1.

nAb	Variant	Counts in competition selection	Counts in reference population	Enrichment Ratio	Minimum nucleotide distance	FDR	p value for FDR < 1
CC.12-1	D405K	249	24	3.5	2	7.7E-07	1.5E-03
CC.12-1	Q414A	566	28	4.5	2	5.0E-13	8.3E-16
CC.12-1	K417A	634	19	5.2	2	5.0E-13	6.8E-25
CC.12-1	K417C	506	21	4.7	3	5.0E-13	1.9E-16
CC.12-1	K417D	358	7	5.8	2	5.0E-13	1.4E-17
CC.12-1	K417E	800	23	5.3	1	5.0E-13	1.0E-31
CC.12-1	K417F	446	12	5.4	3	5.0E-13	6.3E-19
CC.12-1	K417G	1655	54	5.1	2	5.0E-13	1.9E-59
CC.12-1	K417H	432	17	4.8	2	5.0E-13	8.5E-15
CC.12-1	K417I	155	12	3.8	1	1.3E-10	1.6E-03
CC.12-1	K417L	2303	63	5.3	2	5.0E-13	1.1E-90
CC.12-1	K417N	732	19	5.4	1	5.0E-13	1.1E-30
CC.12-1	K417P	1197	11	6.9	2	5.0E-13	3.0E-68
CC.12-1	K417S	1869	45	5.5	2	5.0E-13	1.1E-78

CC.12-1	K417T	1528	38	5.5	1	5.0E-13	1.2E-63
CC.12-1	K417V	787	33	4.7	2	5.0E-13	1.5E-24
CC.12-1	K417W	1427	42	5.2	2	5.0E-13	1.2E-54
CC.12-1	K417Y	523	15	5.3	2	5.0E-13	2.8E-21
CC.12-1	D420A	4199	84	5.8	1	5.0E-13	5.5E-189
CC.12-1	D420C	707	48	4.0	2	7.5E-13	1.1E-13
CC.12-1	D420E	3842	113	5.2	1	5.0E-13	2.7E-144
CC.12-1	D420H	372	34	3.6	1	1.1E-07	3.9E-05
CC.12-1	D420K	584	10	6.0	2	5.0E-13	4.0E-29
CC.12-1	D420L	1885	54	5.3	2	5.0E-13	9.8E-73
CC.12-1	D420M	756	26	5.0	3	5.0E-13	3.9E-27
CC.12-1	D420N	914	24	5.4	1	5.0E-13	1.0E-37
CC.12-1	D420Q	678	24	5.0	2	5.0E-13	4.8E-24
CC.12-1	D420R	4431	110	5.5	2	5.0E-13	1.8E-181
CC.12-1	D420S	1979	49	5.5	2	5.0E-13	4.0E-82
CC.12-1	D420T	733	33	4.6	2	5.0E-13	1.0E-21
CC.12-1	D420W	372	41	3.3	3	5.8E-05	1.5E-03
CC.12-1	D420Y	299	24	3.8	1	6.4E-10	2.4E-05

CC.12-1	Y421A	888	109	3.2	2	1.1E-03	9.5E-05
CC.12-1	Y421C	1952	126	4.1	1	5.0E-13	1.9E-37
CC.12-1	Y421H	1140	27	5.5	1	5.0E-13	5.6E-49
CC.12-1	Y421L	5137	159	5.2	2	5.0E-13	1.1E-186
CC.12-1	Y421N	1262	56	4.6	1	5.0E-13	1.1E-36
CC.12-1	Y421W	3129	156	4.5	2	5.0E-13	1.9E-79
CC.12-1	Q498H	4086	296	3.6	1	1.7E-02	6.9E-30
CC.12-1	Q498Y	1467	147	3.1	2	3.7E-01	2.0E-04
CC.12-1	N501F	7508	617	3.4	2	7.6E-02	3.0E-37
CC.12-1	N501M	9286	519	4.0	2	2.0E-04	4.0E-111
CC.12-1	N501T	10942	890	3.4	1	6.8E-02	3.1E-55
CC.12-1	N501V	12572	885	3.6	2	1.1E-02	1.7E-94
CC.12-1	N501W	4503	305	3.7	3	6.3E-03	2.9E-38
CC.12-1	N501Y	7767	639	3.4	1	7.6E-02	2.5E-38
CC.12-1	Y505W	12149	894	3.6	2	2.1E-02	9.4E-82
CC.12-1	Y508H	1478	113	3.5	1	3.3E-02	1.8E-10
CC.12-1	P527I	467	43	3.3	2	2.1E-01	7.4E-03
CC.12-1	P527M	155	7	4.3	2	1.3E-06	7.5E-04

CC.12-3	Q414A	627	28	4.4	2	5.0E-13	1.1E-13
CC.12-3	Q414G	807	44	4.1	2	5.0E-13	9.8E-14
CC.12-3	T415G	1424	82	4.0	2	1.4E-12	2.3E-21
CC.12-3	K417A	514	19	4.6	2	5.0E-13	1.7E-13
CC.12-3	K417C	496	21	4.4	3	5.0E-13	1.1E-11
CC.12-3	K417D	210	7	4.8	2	5.0E-13	1.0E-06
CC.12-3	K417E	557	23	4.5	1	5.0E-13	3.1E-13
CC.12-3	K417F	344	12	4.7	3	5.0E-13	6.8E-10
CC.12-3	K417G	1439	54	4.6	2	5.0E-13	1.3E-34
CC.12-3	K417H	352	17	4.2	2	5.0E-13	1.0E-07
CC.12-3	K417I	502	12	5.3	1	5.0E-13	2.3E-17
CC.12-3	K417L	2239	63	5.0	2	5.0E-13	1.2E-65
CC.12-3	K417M	983	23	5.3	1	5.0E-13	5.4E-33
CC.12-3	K417N	467	19	4.5	1	5.0E-13	1.8E-11
CC.12-3	K417P	922	11	6.3	2	5.0E-13	3.5E-40
CC.12-3	K417Q	680	28	4.5	1	5.0E-13	7.1E-16
CC.12-3	K417R	1486	84	4.0	1	8.7E-13	8.3E-23
CC.12-3	K417S	1475	45	4.9	2	5.0E-13	1.5E-41

CC.12-3	K417T	1229	38	4.9	1	5.0E-13	1.5E-34
CC.12-3	K417V	1080	33	4.9	2	5.0E-13	8.3E-31
CC.12-3	K417W	1127	42	4.6	2	5.0E-13	1.3E-27
CC.12-3	K417Y	344	15	4.4	2	5.0E-13	2.6E-08
CC.12-3	D420A	2677	84	4.9	1	5.0E-13	1.5E-72
CC.12-3	D420C	619	48	3.6	2	3.0E-07	2.5E-06
CC.12-3	D420E	2875	113	4.5	1	5.0E-13	1.0E-64
CC.12-3	D420K	317	10	4.9	2	5.0E-13	7.6E-10
CC.12-3	D420L	1313	54	4.5	2	5.0E-13	3.1E-29
CC.12-3	D420M	550	26	4.3	3	5.0E-13	1.6E-11
CC.12-3	D420N	595	24	4.5	1	5.0E-13	2.5E-14
CC.12-3	D420Q	410	24	4.0	2	2.6E-12	4.6E-07
CC.12-3	D420R	2769	110	4.5	2	5.0E-13	8.6E-62
CC.12-3	D420S	1061	49	4.3	2	5.0E-13	2.4E-21
CC.12-3	D420T	530	33	3.9	2	4.0E-11	5.1E-08
CC.12-3	D420Y	273	24	3.4	1	2.0E-05	7.1E-03
CC.12-3	Y421A	1030	109	3.1	2	3.1E-03	4.8E-04
CC.12-3	Y421C	1842	126	3.7	1	2.3E-09	1.8E-20

CC.12-3	Y421F	729	80	3.1	1	7.2E-03	6.7E-03
CC.12-3	Y421H	881	27	4.9	1	5.0E-13	2.3E-25
CC.12-3	Y421L	3735	159	4.4	2	5.0E-13	2.6E-77
CC.12-3	Y421N	1039	56	4.1	1	5.0E-13	1.7E-17
CC.12-3	Y421W	3746	156	4.5	2	5.0E-13	2.9E-79
CC.12-3	N460V	315	28	3.4	2	1.1E-01	8.5E-03
CC.12-3	Q498H	3844	296	3.6	1	2.1E-02	4.3E-28
CC.12-3	Q498W	4847	466	3.3	2	2.1E-01	4.7E-17
CC.12-3	Q498Y	1445	147	3.2	2	3.1E-01	4.8E-05
CC.12-3	N501F	9266	617	3.8	2	2.3E-03	7.4E-91
CC.12-3	N501W	4284	305	3.7	3	6.9E-03	1.9E-37
CC.12-3	N501Y	9508	639	3.8	1	2.7E-03	1.9E-91
CC.12-3	Y505W	11672	894	3.6	2	1.9E-02	1.3E-82
CC.12-13	A475K	35	11	3.3	2	3.1E-06	3.7E-02
CC.12-13	N501W	2074	745	3.1	3	1.2E-04	1.3E-35
CC.12-13	N460P	21	8	3.0	2	5.1E-04	1.8E-01
CC.12-13	E484N	21	8	3.0	2	5.1E-04	1.8E-01
CC.12-13	N501F	3378	1311	3.0	2	7.8E-04	3.5E-43

CC.12-13	N501V	4041	1593	3.0	2	1.1E-03	3.5E-48
CC.12-13	N501Y	3028	1339	2.8	1	1.2E-02	2.4E-21
CC.12-13	L455M	19	10	2.6	1	2.1E-01	4.5E-01
CC.12-13	N501T	3053	1677	2.5	1	3.6E-01	2.1E-03
CC.12-13	N501I	2695	1531	2.4	1	5.5E-01	4.9E-02
CC.6-29	A475R	174	6	4.4	2	1.1E-07	5.6E-04
CC.6-29	S477P	472	18	4.3	1	1.8E-06	7.2E-08
CC.6-29	T478L	1562	85	3.7	2	3.4E-03	2.1E-13
CC.6-29	T478Q	239	12	3.9	2	8.4E-04	1.6E-03
CC.6-29	T478R	1421	77	3.8	1	3.2E-03	1.9E-12
CC.6-29	E484I	392	25	3.5	2	3.3E-02	1.9E-03
CC.6-29	E484K	615	36	3.6	1	1.1E-02	1.9E-05
CC.6-29	E484R	1313	87	3.5	2	5.2E-02	1.5E-07
CC.6-29	F486A	741	27	4.3	2	5.3E-07	4.1E-12
CC.6-29	F486G	866	35	4.2	2	7.8E-06	2.1E-12
CC.6-29	F486I	551	29	3.8	1	1.9E-03	5.6E-06
CC.6-29	F486L	2159	103	3.9	1	3.1E-04	1.4E-22
CC.6-29	F486R	325	20	3.6	2	2.1E-02	3.0E-03

CC.6-29	F486S	1207	47	4.2	1	3.1E-06	1.9E-17
CC.6-29	F486V	1421	58	4.2	1	1.0E-05	4.0E-19
CC.6-31	Q493W	176	39	3.2	2	1.8E-05	3.3E-04
CC.6-31	Q493F	166	41	3.1	3	3.0E-04	2.9E-03
CC.6-31	Y505W	3857	1111	2.8	2	8.5E-03	1.6E-22
CC.6-31	L455W	33	10	2.8	1	2.2E-02	2.9E-01
CC.6-31	Q493Y	124	38	2.7	2	2.7E-02	9.2E-02
CC.6-31	N450A	20	8	2.4	2	1.1E+00	6.0E-01

Table S3. Mutations identified in literature. (19–23)

Mutation	Antibody	Germline	Source(PMID)
T345A	2H04	IGHV1-55	33535027
T345N	2H04	IGHV1-55	33535027
T345S	2H04	IGHV1-55	33535027
R346G	SARS2-01		33535027
R346G	2H04	IGHV1-55	33535027
R346K	C135	IGHV3-30	32743579
R346M	C135	IGHV3-30	32743579
R346S	C135	IGHV3-30	32743579
A352D	SARS2-01		33535027
Y369C	COV2-2082	IGHV3-20	32935107
N370K	COV2-2082	IGHV3-20	32935107
N370S	COV2-2082	IGHV3-20	32935107
A372S	COV2-2082	IGHV3-20	32935107
A372T	COV2-2082	IGHV3-20	32935107
A372V	COV2-2082	IGHV3-20	32935107
T376I	COV2-2082	IGHV3-20	32935107
T376I	COV2-2094	IGHV3-20	32935107

K378E	SARS2-31		33535027
K378N	COV2-2677	IGHV4-39	32935107
K378N	COV2-2082	IGHV3-20	32935107
K378N	COV2-2094	IGHV3-20	32935107
K378Q	COV2-2677	IGHV4-39	33535027
K378R	COV2-2677	IGHV4-39	32935107
K378R	COV2-2082	IGHV3-20	32935107
K378R	COV2-2094	IGHV3-20	32935107
P384L	COV2-2677	IGHV4-39	32935107
P384S	COV2-2677	IGHV4-39	32935107
R408I	COV2-2082	IGHV3-20	32935107
R408I	COV2-2094	IGHV3-20	32935107
R408K	COV2-2082	IGHV3-20	32935107
R408K	COV2-2094	IGHV3-20	32935107
R408K	SARS2-31		33535027
R408T	COV2-2082	IGHV3-20	32935107
R408T	COV2-2094	IGHV3-20	32935107
A411S	COV2-2082	IGHV3-20	32935107

K417E	**REGN10933**	**IGHV3-48**	**32540904**
K417N	**COV2-2082**	**IGHV3-20**	**32935107**
K417N	**COV2-2094**	**IGHV3-20**	**32935107**
K417R	**COV2-2082**	**IGHV3-20**	**32935107**
K417R	**COV2-2094**	**IGHV3-20**	**32935107**
A435S	**COV2-2094**	**IGHV3-20**	**32935107**
D614G+A435S	**H014**		**32730807**
N439K	**H00S022**		**32730807**
N440K	**C135**	**IGHV3-30**	**32743579**
L441R	**2H04**	**IGHV1-55**	**33535027**
K444E	**2H04**	**IGHV1-55**	**33535027**
K444E	**SARS2-38**		**33535027**
K444E	**SARS2-22**		**33535027**
K444N	**SARS2-38**		**33535027**
K444R	**SARS2-22**		**33535027**
K444Q	**REGN10934**	**IGHV3-15**	**32540904**
K444Q	**REGN10987**	**IGHV3-30**	**32540904**
K444R	**SARS2-22**		**33535027**

V445A	**REGN10987**	**IGHV3-30**	**32540904**
V445A	**COV2-2499**	**IGHV4-39**	**32935107**
V445F	**COV2-2499**	**IGHV4-39**	**32935107**
V445G	**SARS2-22**		**33535027**
V445I	**COV2-2499**	**IGHV4-39**	**32935107**
G446A	**COV2-2096**	**IGHV1-8**	**32935107**
G446A	**COV2-2499**	**IGHV4-39**	**32935107**
G446D	**SARS2-02**		**33535027**
G446D	**SARS2-32**		**33535027**
G446D	**SARS2-38**		**33535027**
G446D	**SARS2-22**		**33535027**
G446S	**COV2-2096**	**IGHV1-8**	**32935107**
G446S	**COV2-2499**	**IGHV4-39**	**32935107**
G446V	**COV2-2096**	**IGHV1-8**	**32935107**
G446V	**COV2-2499**	**IGHV4-39**	**32935107**
G446V	**SARS2-02**		**33535027**
N450D	**SARS2-07**		**33535027**

N450K	**SARS2-32**		**33535027**
N450Y	**SARS2-32**		**33535027**
L452M	**COV2-2096**	**IGHV1-8**	**32935107**
L452R	**COV2-2096**	**IGHV1-8**	**32935107**
L452R	**X593**		**32730807**
L452R	**P2B-2F6**	**IGHV4-38**	**32730807**
L452R	**SARS2-01**		**33535027**
L452R	**SARS2-32**		**33535027**
Y453F	**REGN10933**	**IGHV3-48**	**32540904**
L455F	**REGN10933**	**IGHV3-48**	**32540904**
K458Q	**SARS2-66**		**33535027**
I472V	**COV2-2479**	**IGHV1-69**	**32935107**
D614G+I472V	**X593**		**32730807**
Q474P	**SARS2-34**		**33535027**
A475V	**157**		**32730807**
A475V	**247**		**32730807**
A475V	**CB6**	**IGHV3-66**	**32730807**
A475V	**P2C-1F11**	**IGHV3-66**	**32730807**

A475V	**B38**	**IGHV3-53**	**32730807**
A475V	**CA1**	**IGHV1-18**	**32730807**
A475V	**COV2-2165**	**IGHV3-66**	**32935107**
A475V	**COV2-2832**	**IGHV3-66**	**32935107**
G476D	**SARS2-21**		**33535027**
G476D	**SARS2-34**		**33535027**
G476D	**SARS2-71**		**33535027**
G476S	**SARS2-21**		**33535027**
S477G	**SARS2-16**		**33535027**
S477G	**SARS2-07**		**33535027**
S477G	**SARS2-19**		**33535027**
S477G	**SARS2-34**		**33535027**
S477G	**SARS2-58**		**33535027**
S477G	**SARS2-71**		**33535027**
S477I	**SARS2-58**		**33535027**
S477N	**SARS2-16**		**33535027**
S477N	**SARS2-07**		**33535027**

S477N	**SARS2-19**		**33535027**
S477N	**SARS2-34**		**33535027**
S477N	**SARS2-58**		**33535027**
P477L	**SARS2-07**		**33535027**
S477R	**SARS2-07**		**33535027**
S477R	**SARS2-16**		**33535027**
S477R	**SARS2-23**		**33535027**
S477R	**SARS2-34**		**33535027**
T478I	**SARS2-19**		**33535027**
T478I	**SARS2-21**		**33535027**
T478I	**SASRS2-71**		**33535027**
T478P	**SASRS2-71**		**33535027**
P479L	**SARS2-34**		**33535027**
P479L	**SARS2-71**		**33535027**
P479S	**SARS2-21**		**33535027**
V483A	**X593**		**32730807**
V483A	**P2B-2F6**	**IGHV4-38**	**32730807**

V483F	SARS2-23		33535027
V483G	SARS2-23		33535027
E484A	2B04	IGHV2-9	33535027
E484A	COV2-2832	IGHV3-66	32935107
E484A	COV2-2479	IGHV1-69	32935107
E484A	COV2-2050	IGHV1-2	32935107
E484A	1B07	IGHV2-9	33535027
E484A	COV2-2096	IGHV1-8	32935107
E484D	COV2-2832	IGHV3-66	32935107
E484D	COV2-2479	IGHV1-69	32935107
E484D	COV2-2050	IGHV1-2	32935107
E484D	COV2-2096	IGHV1-8	32935107
E484D	1B07	IGHV2-9	33535027
E484D	SARS2-23		33535027
E484D	SARS2-66		33535027
E484G	1B07	IGHV2-9	33535027
E484K	COV2-2832	IGHV3-66	32935107
E484K	COV2-2479	IGHV1-69	32935107

E484K	**COV2-2050**	**IGHV1-2**	**32935107**
E484K	**COV2-2096**	**IGHV1-8**	**32935107**
E484K	**REGN10989**	**IGHV1-2**	**32540904**
E484K	**REGN10933**	**IGHV3-48**	**32540904**
E484K	**REGN10934**	**IGHV3-15**	**32540904**
E484K	**REGN10989/10934**	**IGHV1-2/IGHV3-15**	**32540904**
E484K	**2B04**	**IGHV2-9**	**33535027**
E484K	**1B07**	**IGHV2-9**	**33535027**
E484K	**SARS2-02**		**33535027**
E484K	**SARS2-32**		**33535027**
E484K	**SARS2-58**		**33535027**
E484K	**C121**	**IGHV1-2**	**32743579**
E484K	**C144**	**IGHV3-53**	**32743579**
E484Q	**COV2-2832**	**IGHV3-66**	**32935107**
E484Q	**COV2-2479**	**IGHV1-69**	**32935107**
E484Q	**COV2-2050**	**IGHV1-2**	**32935107**
E484Q	**COV2-2096**	**IGHV1-8**	**32935107**
G485D	**REGN10989**	**IGHV1-2**	**32540904**

F486S	**2B04**	**IGHV2-9**	**33535027**
F486S	**SARS2-21**		**33535027**
F486V	**REGN10989**	**IGHV1-2**	**32540904**
F486V	**REGN10933**	**IGHV3-48**	**32540904**
F486V	**SARS2-58**		**33535027**
F486V	**SARS2-71**		**33535027**
F486L	**COV2-2832**	**IGHV3-66**	**32935107**
F486L	**SARS2-21**		**33535027**
F486Y	**1B07**	**IGHV2-9**	**33535027**
F490P	**REGN10989**	**IGHV1-2**	**32540904**
F490P	**REGN10934**	**IGHV3-15**	**32540904**
F490P	**REGN10989/10934**	**IGHV1-2/IGHV3-15**	**32540904**
F490L	**X593**		**32730807**
F490L	**261-262**		**32730807**
F490L	**H4**	**IGHV1-2**	**32730807**
F490L	**P2B-2F6**	**IGHV4-38**	**32730807**
F490L	**COV2-2479**	**IGHV1-69**	**32935107**

F490L	**COV2-2050**	**IGHV1-2**	**32935107**
F490L	**COV2-2096**	**IGHV1-8**	**32935107**
F490L	**SARS2-66**		**33535027**
F490L	**C121**	**IGHV1-2**	**32743579**
F490S	**COV2-2479**	**IGHV1-69**	**32935107**
F490S	**COV2-2050**	**IGHV1-2**	**32935107**
F490S	**COV2-2096**	**IGHV1-8**	**32935107**
F490S	**SARS2-32**		**33535027**
Q493K	**REGN10989**	**IGHV1-2**	**32540904**
Q493K	**REGN10933**	**IGHV3-48**	**32540904**
Q493K	**REGN10989/10934**	**IGHV1-2/IGHV3-15**	**32540904**
Q493K	**C144**	**IGHV3-53**	**32743579**
Q493R	**C144**	**IGHV3-53**	**32743579**
Q493K	**C121**	**IGHV1-2**	**32743579**
S494L	**COV2-2096**	**IGHV1-8**	**32935107**
S494P	**COV2-2096**	**IGHV1-8**	**32935107**
S494P	**SARS2-01**		**33535027**
P499H	**COV2-2499**	**IGHV4-39**	**32935107**

P499R	**COV2-2499**	**IGHV4-39**	**32935107**
P499S	**COV2-2499**	**IGHV4-39**	**32935107**
G504D	**SARS2-31**		**33535027**
Y508H	**H014**		**32730807**

Table S4. List of plasmids used in this study.

Name	Description	*E. coli* Marker	Yeast marker	Source
pUC19-S-ecto-B	S ectodomain fragment positions 501-814 with BsaI sites for assembly and BbvCI site	Amp		This study
pUC19-S-ecto-C-Nterm	S ectodomain fragment positions 815-1198 with a C-terminal T4 fibritin trimerization domain with BsaI sites for assembly and BbvCI site	Amp		This study
pUC19-S-ecto-A-Nterm-KanR	S ectodomain fragment positions 13-500 with BsaI sites for assembly and BbvCI site	Kan		This study
pUC19-S-ecto-Nterm	S ectodomain for N-terminal YSD	Kan		This study
pJS697	YSD vector backbone (C-terminal fusion) for in vivo HR	Kan	TRP1	This study
pJS698	YSD vector backbone (N-terminal fusion) for in vivo HR	Kan	TRP1	This study
pJS699	S-RBD(333-537)-N343Q	Kan		Banach et al., 2021 (4)

Table S5. List of primers used.

Name	description	sequence
Downcmyc	Secondary primer for nicking mutagenesis	CAAGTCCTCTTCAGAAATAAGCTTTG
M13F	Secondary primer for oligo pool mutagenesis	TGTAAAACGACGGCCAGT
MBK-175	KanR-fwd	CAATAATATTGAAAAAGGAAGAGT
MBK-176	KanR-rev	ATGAGTAAACTTGGTCTGACAGTT
MBK-177	A-pUC19-fwd	AACTGTCAGACCAAGTTTACTCAT
MBK-178	A-pUC19-rev	ACTCTTCCTTTTTCAATATTATTG
MBK-180	DS-tile1-fwd	GTTCAGAGTTCTACAGTCCGACGATCACACGTGGTGTTTATTACCCT
MBK-181	DS-tile1-rev	CCTTGGCACCCGAGAATTCCACATAAGAAAAGGCTGAGAGACATA
MBK-301	DS-tile2-fwd	GTTCAGAGTTCTACAGTCCGACGATCCTTAGGGAATTTGTGTTTAAG
MBK-302	DS-tile2-rev	CCTTGGCACCCGAGAATTCCAAACTTCACCAAAAGGGCACAA
MBK-303	DS-tile3-fwd	GTTCAGAGTTCTACAGTCCGACGATCAGGAAGAGAATCAGCAACTGT
MBK-304	DS-tile3-rev	CCTTGGCACCCGAGAATTCCAATGATTGTAAAGGAAAGTAACA
MBK-305	DS-tile4-fwd	GTTCAGAGTTCTACAGTCCGACGATCAGTAGTAGTACTTTCTTTTGAACTT
MBK-306	DS-tile4-rev	CCTTGGCACCCGAGAATTCCAGGTGTAATGTCAAGAATCTCAAG
MBK-307	DS-tile5-fwd	GTTCAGAGTTCTACAGTCCGACGATCGACTCACTTTCTTCCACAGCA
MBK-308	DS-tile5-rev	CCTTGGCACCCGAGAATTCCAAGCTCTGATTTCTGCAGCTCT

PJS-P2192	**pETCON-NK-BsaI-C-term-fwd**	TGTTATGGAGCGGGTCTCAGGGGGCGGATCCGAA
PJS-P2193	**pETCON-NK-BsaI-C-term-rev**	ACGTTCAGTGATGGTCTCTACTAGCCTGCAGAGC
PJS-P2194	**pETCON-NK-BsaI-N-term-fwd**	TGTTATGGAGCGGGTCTCACAGGAACTGACAACTATATGC
PJS-P2195	**pETCON-NK-BsaI-N-term-rev**	ACGTTCAGTGATGGTCTCTGAAAATATTGAAAAACAGCGAAGTAA
RBD_1	T333-NNK	TGGAGGCGGTAGCGGAGGCGGAGGGTCGNNKAACTTGTGCCCTTTTGGTGAAGTTTTTC
RBD_2	N334-NNK	AGGCGGTAGCGGAGGCGGAGGGTCGACANNKTTGTGCCCTTTTGGTGAAGTTTTTCAAG
RBD_3	L335-NNK	CGGTAGCGGAGGCGGAGGGTCGACAAACNNKTGCCCTTTTGGTGAAGTTTTTCAAGCCA
RBD_4	G339-NNK	CGGAGGGTCGACAAACTTGTGCCCTTTTNNKGAAGTTTTTCAAGCCACCAGATTTGCAT
RBD_5	E340-NNK	AGGGTCGACAAACTTGTGCCCTTTTGGTNNKGTTTTTCAAGCCACCAGATTTGCATCTG
RBD_6	A344-NNK	CTTGTGCCCTTTTGGTGAAGTTTTTCAANNKACCAGATTTGCATCTGTTTATGCTTGGA
RBD_7	T345-NNK	GTGCCCTTTTGGTGAAGTTTTTCAAGCCNNKAGATTTGCATCTGTTTATGCTTGGAACA
RBD_8	R346-NNK	CCCTTTTGGTGAAGTTTTTCAAGCCACCNNKTTTGCATCTGTTTATGCTTGGAACAGGA
RBD_9	S349-NNK	TGAAGTTTTTCAAGCCACCAGATTTGCANNKGTTTATGCTTGGAACAGGAAGAGAATCA
RBD_10	Y351-NNK	TTTTCAAGCCACCAGATTTGCATCTGTTNNKGCTTGGAACAGGAAGAGAATCAGCAACT
RBD_11	A352-NNK	TCAAGCCACCAGATTTGCATCTGTTTATNNKTGGAACAGGAAGAGAATCAGCAACTGTG
RBD_12	N354-NNK	CACCAGATTTGCATCTGTTTATGCTTGGNNKAGGAAGAGAATCAGCAACTGTGTTGCTG
RBD_13	K356-NNK	ATTTGCATCTGTTTATGCTTGGAACAGGNNKAGAATCAGCAACTGTGTTGCTGATTATT

RBD_14	R357-NNK	TGCATCTGTTTATGCTTGGAACAGGAAGNNKATCAGCAACTGTGTTGCTGATTATTCTG
RBD_15	I358-NNK	ATCTGTTTATGCTTGGAACAGGAAGAGANNKAGCAACTGTGTTGCTGATTATTCTGTCC
RBD_16	S359-NNK	TGTTTATGCTTGGAACAGGAAGAGAATCNNKAACTGTGTTGCTGATTATTCTGTCCTAT
RBD_17	N360-NNK	TTATGCTTGGAACAGGAAGAGAATCAGCNNKTGTGTTGCTGATTATTCTGTCCTATATA
RBD_18	V362-NNK	TTGGAACAGGAAGAGAATCAGCAACTGTNNKGCTGATTATTCTGTCCTATATAATTCCG
RBD_19	A363-NNK	GAACAGGAAGAGAATCAGCAACTGTGTTNNKGATTATTCTGTCCTATATAATTCCGCAT
RBD_20	D364-NNK	CAGGAAGAGAATCAGCAACTGTGTTGCTNNKTATTCTGTCCTATATAATTCCGCATCAT
RBD_21	S366-NNK	GAGAATCAGCAACTGTGTTGCTGATTATNNKGTCCTATATAATTCCGCATCATTTTCCA
RBD_22	V367-NNK	AATCAGCAACTGTGTTGCTGATTATTCTNNKCTATATAATTCCGCATCATTTTCCACTT
RBD_23	N370-NNK	CTGTGTTGCTGATTATTCTGTCCTATATNNKTCCGCATCATTTTCCACTTTTAAGTGTT
RBD_24	A372-NNK	TGCTGATTATTCTGTCCTATATAATTCCNNKTCATTTTCCACTTTTAAGTGTTATGGAG
RBD_25	S373-NNK	TGATTATTCTGTCCTATATAATTCCGCANNKTTTTCCACTTTTAAGTGTTATGGAGTGT
RBD_26	S375-NNK	TTCTGTCCTATATAATTCCGCATCATTTNNKACTTTTAAGTGTTATGGAGTGTCTCCTA
RBD_27	T376-NNK	TGTCCTATATAATTCCGCATCATTTTCCNNKTTTAAGTGTTATGGAGTGTCTCCTACTA
RBD_28	F377-NNK	CCTATATAATTCCGCATCATTTTCCACTNNKAAGTGTTATGGAGTGTCTCCTACTAAAT
RBD_29	K378-NNK	ATATAATTCCGCATCATTTTCCACTTTTNNKTGTTATGGAGTGTCTCCTACTAAATTAA
RBD_30	Y380-NNK	TTCCGCATCATTTTCCACTTTTAAGTGTNNKGGAGTGTCTCCTACTAAATTAAATGATC
RBD_31	G381-NNK	CGCATCATTTTCCACTTTTAAGTGTTATNNKGTGTCTCCTACTAAATTAAATGATCTCT

RBD_32	V382-NNK	ATCATTTTCCACTTTTAAGTGTTATGGANNKTCTCCTACTAAATTAAATGATCTCTGCT
RBD_33	S383-NNK	ATTTTCCACTTTTAAGTGTTATGGAGTGNNKCCTACTAAATTAAATGATCTCTGCTTTA
RBD_34	P384-NNK	TTCCACTTTTAAGTGTTATGGAGTGTCTNNKACTAAATTAAATGATCTCTGCTTTACTA
RBD_35	T385-NNK	CACTTTTAAGTGTTATGGAGTGTCTCCTNNKAAATTAAATGATCTCTGCTTTACTAATG
RBD_36	K386-NNK	TTTTAAGTGTTATGGAGTGTCTCCTACTNNKTTAAATGATCTCTGCTTTACTAATGTCT
RBD_37	N388-NNK	GTGTTATGGAGTGTCTCCTACTAAATTANNKGATCTCTGCTTTACTAATGTCTATGCAG
RBD_38	D389-NNK	TTATGGAGTGTCTCCTACTAAATTAAATNNKCTCTGCTTTACTAATGTCTATGCAGATT
RBD_39	L390-NNK	TGGAGTGTCTCCTACTAAATTAAATGATNNKTGCTTTACTAATGTCTATGCAGATTCAT
RBD_40	N394-NNK	TACTAAATTAAATGATCTCTGCTTTACTNNKGTCTATGCAGATTCATTTGTAATTAGAG
RBD_41	Y396-NNK	ATTAAATGATCTCTGCTTTACTAATGTCNNKGCAGATTCATTTGTAATTAGAGGTGATG
RBD_42	D405-NNK	CTATGCAGATTCATTTGTAATTAGAGGTNNKGAAGTCAGACAAATCGCTCCAGGGCAAA
RBD_43	R408-NNK	TTCATTTGTAATTAGAGGTGATGAAGTCNNKCAAATCGCTCCAGGGCAAACTGGAAAGA
RBD_44	A411-NNK	AATTAGAGGTGATGAAGTCAGACAAATCNNKCCAGGGCAAACTGGAAAGATTGCTGATT
RBD_45	P412-NNK	TAGAGGTGATGAAGTCAGACAAATCGCTNNKGGGCAAACTGGAAAGATTGCTGATTATA
RBD_46	G413-NNK	AGGTGATGAAGTCAGACAAATCGCTCCANNKCAAACTGGAAAGATTGCTGATTATAATT
RBD_47	Q414-NNK	TGATGAAGTCAGACAAATCGCTCCAGGGNNKACTGGAAAGATTGCTGATTATAATTATA
RBD_48	T415-NNK	TGAAGTCAGACAAATCGCTCCAGGGCAANNKGGAAAGATTGCTGATTATAATTATAAAT
RBD_49	K417-NNK	CAGACAAATCGCTCCAGGGCAAACTGGANNKATTGCTGATTATAATTATAAATTACCAG

RBD_50	D420-NNK	CGCTCCAGGGCAAACTGGAAAGATTGCTNNKTATAATTATAAATTACCAGATGATTTTA
RBD_51	Y421-NNK	TCCAGGGCAAACTGGAAAGATTGCTGATNNKAATTATAAATTACCAGATGATTTTACAG
RBD_52	K424-NNK	AACTGGAAAGATTGCTGATTATAATTATNNKTTACCAGATGATTTTACAGGCTGCGTTA
RBD_53	P426-NNK	AAAGATTGCTGATTATAATTATAAATTANNKGATGATTTTACAGGCTGCGTTATAGCTT
RBD_54	D427-NNK	GATTGCTGATTATAATTATAAATTACCANNKGATTTTACAGGCTGCGTTATAGCTTGGA
RBD_55	D428-NNK	TGCTGATTATAATTATAAATTACCAGATNNKTTTACAGGCTGCGTTATAGCTTGGAATT
RBD_56	T430-NNK	TTATAATTATAAATTACCAGATGATTTTNNKGGCTGCGTTATAGCTTGGAATTCTAACA
RBD_57	N437-NNK	TGATTTTACAGGCTGCGTTATAGCTTGGNNKTCTAACAATCTTGATTCTAAGGTTGGTG
RBD_58	N439-NNK	TACAGGCTGCGTTATAGCTTGGAATTCTNNKAATCTTGATTCTAAGGTTGGTGGTAATT
RBD_59	N440-NNK	AGGCTGCGTTATAGCTTGGAATTCTAACNNKCTTGATTCTAAGGTTGGTGGTAATTATA
RBD_60	L441-NNK	CTGCGTTATAGCTTGGAATTCTAACAATNNKGATTCTAAGGTTGGTGGTAATTATAATT
RBD_61	K444-NNK	AGCTTGGAATTCTAACAATCTTGATTCTNNKGTTGGTGGTAATTATAATTACCTGTATA
RBD_62	V445-NNK	TTGGAATTCTAACAATCTTGATTCTAAGNNKGGTGGTAATTATAATTACCTGTATAGAT
RBD_63	G446-NNK	GAATTCTAACAATCTTGATTCTAAGGTTNNKGGTAATTATAATTACCTGTATAGATTGT
RBD_64	G447-NNK	TTCTAACAATCTTGATTCTAAGGTTGGTNNKAATTATAATTACCTGTATAGATTGTTTA
RBD_65	N448-NNK	TAACAATCTTGATTCTAAGGTTGGTGGTNNKTATAATTACCTGTATAGATTGTTTAGGA
RBD_66	Y449-NNK	CAATCTTGATTCTAAGGTTGGTGGTAATNNKAATTACCTGTATAGATTGTTTAGGAAGT
RBD_67	N450-NNK	TCTTGATTCTAAGGTTGGTGGTAATTATNNKTACCTGTATAGATTGTTTAGGAAGTCTA

RBD_68	L452-NNK	TTCTAAGGTTGGTGGTAATTATAATTACNNKTATAGATTGTTTAGGAAGTCTAATCTCA
RBD_69	L455-NNK	TGGTGGTAATTATAATTACCTGTATAGANNKTTTAGGAAGTCTAATCTCAAACCTTTTG
RBD_70	F456-NNK	TGGTAATTATAATTACCTGTATAGATTGNNKAGGAAGTCTAATCTCAAACCTTTTGAGA
RBD_71	R457-NNK	TAATTATAATTACCTGTATAGATTGTTTNNKAAGTCTAATCTCAAACCTTTTGAGAGAG
RBD_72	K458-NNK	TTATAATTACCTGTATAGATTGTTTAGGNNKTCTAATCTCAAACCTTTTGAGAGAGATA
RBD_73	S459-NNK	TAATTACCTGTATAGATTGTTTAGGAAGNNKAATCTCAAACCTTTTGAGAGAGATATTT
RBD_74	N460-NNK	TTACCTGTATAGATTGTTTAGGAAGTCTNNKCTCAAACCTTTTGAGAGAGATATTTCAA
RBD_75	K462-NNK	GTATAGATTGTTTAGGAAGTCTAATCTCNNKCCTTTTGAGAGAGATATTTCAACTGAAA
RBD_76	P463-NNK	TAGATTGTTTAGGAAGTCTAATCTCAAANNKTTTGAGAGAGATATTTCAACTGAAATCT
RBD_77	F464-NNK	ATTGTTTAGGAAGTCTAATCTCAAACCTNNKGAGAGAGATATTTCAACTGAAATCTATC
RBD_78	E465-NNK	GTTTAGGAAGTCTAATCTCAAACCTTTTNNKAGAGATATTTCAACTGAAATCTATCAGG
RBD_79	R466-NNK	TAGGAAGTCTAATCTCAAACCTTTTGAGNNKGATATTTCAACTGAAATCTATCAGGCCG
RBD_80	I468-NNK	GTCTAATCTCAAACCTTTTGAGAGAGATNNKTCAACTGAAATCTATCAGGCCGGTAGCA
RBD_81	S469-NNK	TAATCTCAAACCTTTTGAGAGAGATATTNNKACTGAAATCTATCAGGCCGGTAGCACAC
RBD_82	T470-NNK	TCTCAAACCTTTTGAGAGAGATATTTCANNKGAAATCTATCAGGCCGGTAGCACACCTT
RBD_83	E471-NNK	CAAACCTTTTGAGAGAGATATTTCAACTNNKATCTATCAGGCCGGTAGCACACCTTGTA
RBD_84	Y473-NNK	TTTTGAGAGAGATATTTCAACTGAAATCNNKCAGGCCGGTAGCACACCTTGTAATGGTG
RBD_85	Q474-NNK	TGAGAGAGATATTTCAACTGAAATCTATNNKGCCGGTAGCACACCTTGTAATGGTGTTG

RBD_86	A475-NNK	GAGAGATATTTCAACTGAAATCTATCAGNNKGGTAGCACACCTTGTAATGGTGTTGAAG
RBD_87	S477-NNK	TATTTCAACTGAAATCTATCAGGCCGGTNNKACACCTTGTAATGGTGTTGAAGGTTTTA
RBD_88	T478-NNK	TTCAACTGAAATCTATCAGGCCGGTAGCNNKCCTTGTAATGGTGTTGAAGGTTTTAATT
RBD_89	P479-NNK	AACTGAAATCTATCAGGCCGGTAGCACANNKTGTAATGGTGTTGAAGGTTTTAATTGTT
RBD_90	N481-NNK	AATCTATCAGGCCGGTAGCACACCTTGTNNKGGTGTTGAAGGTTTTAATTGTTACTTTC
RBD_91	G482-NNK	CTATCAGGCCGGTAGCACACCTTGTAATNNKGTTGAAGGTTTTAATTGTTACTTTCCTT
RBD_92	V483-NNK	TCAGGCCGGTAGCACACCTTGTAATGGTNNKGAAGGTTTTAATTGTTACTTTCCTTTAC
RBD_93	E484-NNK	GGCCGGTAGCACACCTTGTAATGGTGTTNNKGGTTTTAATTGTTACTTTCCTTTACAAT
RBD_94	G485-NNK	CGGTAGCACACCTTGTAATGGTGTTGAANNKTTTAATTGTTACTTTCCTTTACAATCAT
RBD_95	F486-NNK	TAGCACACCTTGTAATGGTGTTGAAGGTNNKAATTGTTACTTTCCTTTACAATCATATG
RBD_96	N487-NNK	CACACCTTGTAATGGTGTTGAAGGTTTTNNKTGTTACTTTCCTTTACAATCATATGGTT
RBD_97	Y489-NNK	TTGTAATGGTGTTGAAGGTTTTAATTGTNNKTTTCCTTTACAATCATATGGTTTCCAAC
RBD_98	F490-NNK	TAATGGTGTTGAAGGTTTTAATTGTTACNNKCCTTTACAATCATATGGTTTCCAACCCA
RBD_99	L492-NNK	TGTTGAAGGTTTTAATTGTTACTTTCCTNNKCAATCATATGGTTTCCAACCCACTAATG
RBD_100	Q493-NNK	TGAAGGTTTTAATTGTTACTTTCCTTTANNKTCATATGGTTTCCAACCCACTAATGGTG
RBD_101	S494-NNK	AGGTTTTAATTGTTACTTTCCTTTACAANNKTATGGTTTCCAACCCACTAATGGTGTTG
RBD_102	Q498-NNK	TTACTTTCCTTTACAATCATATGGTTTCNNKCCCACTAATGGTGTTGGTTACCAACCAT
RBD_103	P499-NNK	CTTTCCTTTACAATCATATGGTTTCCAANNKACTAATGGTGTTGGTTACCAACCATACA

RBD_104	T500-NNK	TCCTTTACAATCATATGGTTTCCAACCCNNKAATGGTGTTGGTTACCAACCATACAGAG
RBD_105	N501-NNK	TTTACAATCATATGGTTTCCAACCCACTNNKGGTGTTGGTTACCAACCATACAGAGTAG
RBD_106	V503-NNK	ATCATATGGTTTCCAACCCACTAATGGTNNKGGTTACCAACCATACAGAGTAGTAGTAC
RBD_107	G504-NNK	ATATGGTTTCCAACCCACTAATGGTGTTNNKTACCAACCATACAGAGTAGTAGTACTTT
RBD_108	Y505-NNK	TGGTTTCCAACCCACTAATGGTGTTGGTNNKCAACCATACAGAGTAGTAGTACTTTCTT
RBD_109	Q506-NNK	TTTCCAACCCACTAATGGTGTTGGTTACNNKCCATACAGAGTAGTAGTACTTTCTTTTG
RBD_110	Y508-NNK	ACCCACTAATGGTGTTGGTTACCAACCANNKAGAGTAGTAGTACTTTCTTTTGAACTTC
RBD_111	E516-NNK	ACCATACAGAGTAGTAGTACTTTCTTTTNNKCTTCTACATGCACCAGCAACTGTTTGTG
RBD_112	L517-NNK	ATACAGAGTAGTAGTACTTTCTTTTGAANNKCTACATGCACCAGCAACTGTTTGTGGAC
RBD_113	L518-NNK	CAGAGTAGTAGTACTTTCTTTTGAACTTNNKCATGCACCAGCAACTGTTTGTGGACCTA
RBD_114	H519-NNK	AGTAGTAGTACTTTCTTTTGAACTTCTANNKGCACCAGCAACTGTTTGTGGACCTAAAA
RBD_115	A520-NNK	AGTAGTACTTTCTTTTGAACTTCTACATNNKCCAGCAACTGTTTGTGGACCTAAAAAGT
RBD_116	P521-NNK	AGTACTTTCTTTTGAACTTCTACATGCANNKGCAACTGTTTGTGGACCTAAAAAGTCTA
RBD_117	A522-NNK	ACTTTCTTTTGAACTTCTACATGCACCANNKACTGTTTGTGGACCTAAAAAGTCTACTA
RBD_118	T523-NNK	TTCTTTTGAACTTCTACATGCACCAGCANNKGTTTGTGGACCTAAAAAGTCTACTAATT
RBD_119	P527-NNK	TCTACATGCACCAGCAACTGTTTGTGGANNKAAAAAGTCTACTAATTTGGTTAAAAACA
IFU-104	L1_Inner_FWD	gttcagagttctacagtccgacgatcTGGAGGAGGCTCTGG
IFU-105	L1_Inner_REV	ccttggcacccgagaattccaCCAAGCTATAACGCAGCC

IFU-106	**L2_Inner_FWD**	**gttcagagttctacagtccgacgatcGGCTGCGTTATAGCTTGG**
IFU-107	**L2_Inner_REV**	**ccttggcacccgagaattccaGCCCCCTTTGTTTTAACCAA**
	Forward Outer Primer	**AATGATACGGCGACCACCGAGATCTACACGTTCAGAGTTCTACAGTCCGACGATC**
	Reverse Outer Primer	**CAAGCAGAAGACGGCATACGAGATNNNNNNGTGACTGGAGTTCCTTGGCACCCGAGAATTCCA** **Where NNNNNN is the indexing barcode, for full sequences refer to** (24)

Data S1.
Processed files for all nAb escape mutant identification using S RBD.

Data S2.
Spike mutational designs and DNA sequences encoded in the oligo pool library.

Data S3.
Processed Spike ectodomain library results for sorting against ACE2, CR3022.